Measurement 176 (2021) 109193

Contents lists available at ScienceDirect

Measurement

journal homepage: www.elsevier.com/locate/measurement

Review of electromagnetic waves-based distance measurement technologies for remote monitoring of civil engineering structures

Yiming Liu, Yi Bao *

Department of Civil, Environmental and Ocean Engineering, Stevens Institute of Technology, Hoboken, NJ 07030, USA

ARTICLE INFO

Keywords:
Computer vision
Condition assessment
Electromagnetic wave
Global navigation satellite system
Laser-based measurement
Microwave radar
Remote sensing

ABSTRACT

Measuring distance is essential for health monitoring and condition assessment of civil engineering structures. This paper reviews recent advances in remote sensing technologies for measuring distance based on electromagnetic waves. Specifically, four families of technologies are reviewed, which are the Global Navigation Satellite Systems, microwave radars, laser-based methods, and vision-based methods. The reviewed content covers the measurement principles, signal processing methods, state-of-the-art applications, and key performance metrics. The investigated performance includes the measurement accuracy, sampling frequency, operating distance, robustness to the environment, and compatibility with autonomous platforms. Existing inconsistent viewpoints concerning the performance are discussed. Based on the features of different technologies, a decision tree is presented to facilitate selection of appropriate methods for intended applications. This research is expected to promote development and applications of remote sensing technologies for facilitating condition assessment of engineering structures.

1. Introduction

According to the ASCE's 2017 infrastructure report card, about 40% of 614,387 bridges in the U.S. are 50 years or older [1]. It is estimated that 188 million trips are taken across structurally deficient bridges every day [2]. An additional $206 billion annual investment in infrastructure maintenance is needed to close the 10-year funding gap [1]. The gap results in a loss of $4 trillion in gross domestic product, 2.5 million jobs, and $3,400 in annual disposable income for each household in the U.S. [2]. Under such a circumstance, it is essential to prioritize infrastructure for rehabilitation based on the health condition. Thus, it is significant to assess structural condition to provide high-confidence data to decision makers and stakeholders (e.g., government agencies, industrial companies, and infrastructure users) for cost-effective maintenance [3].

Measurement of distance is important for the safety and efficiency of the construction, operation, and maintenance of civil infrastructure [4,5]. In the construction stage, measuring distance is important for quality control because the geometry and deformation of structures can be precisely determined to inform the structural conditions [10]. Therefore, distance measurement has been a common method adopted in construction. In addition, measurement of distance becomes more relevant when robotic systems are used in construction. In Construction 4.0 era [6], it is projected that more robotic systems will be utilized to significantly transform the existing construction practices. Examples of construction methods based on robotic systems include large-scale three-dimensional (3D) printing [7], modular construction [5], and digital twinning [8,9]. The robotic systems need appropriate measurements of distance for navigation and operation in construction [11,12]. In the operation stage, measuring distance is an effective method to quantify structural responses under various effects [4], such as vehicle loads, temperature variations, settlement of foundation, and ground motion. Large structural deformations may significantly affect the safety and ride comfort of vehicles [13]. Based on the distance measurement result, the structural behaviors can be evaluated to support the data-driven decision making for maintenance of structures, such as prioritization of structures for repairing or retrofitting.

Traditionally, distance was measured using wired sensors, such as linear variable differential transformers [14,15], electromechanical dial gauges [16], hydrostatic level meters [17,18], and inclinometers [19,20], which involved costly fabrication, installation, operation, and maintenance [21]. Since each sensor only measures a local spot, a large number of sensors and wires are needed to monitor a real structure (e.g., bridge, building). To overcome the limitations of wired sensors, wireless

* Corresponding author.
E-mail address: yi.bao@stevens.edu (Y. Bao).

https://doi.org/10.1016/j.measurement.2021.109193
Received 4 January 2021; Received in revised form 8 February 2021; Accepted 15 February 2021
Available online 21 February 2021

measurement technologies have been developed based on electromagnetic (EM) waves. Representative families of the technologies include Global Navigation Satellite Systems (GNSS) [22,23], microwave radar [24,25], laser-based methods [26,27], and computer vision-based methods [28,29]. These wireless measurement technologies have demonstrated common advantages, such as remote sensing [23], all-weather capability [24], 3D information [27], high accuracy [25], and high resolution [25].

Because of the importance of distance measurement, recent reviews provided valuable insights into the four families of technologies. Yu et al. [30] reviewed the prior development of GNSS technologies regarding the sensors, noise mitigation methods, and parameter identification methods. Feng et al. [31] reviewed computer vision-based technologies for measuring structural vibrations, including sensing performance and measurement errors. Although the existing studies have greatly advanced the capability of distance measurement, there are still limitations. First, given the many different types of technologies, it remains unknown how to select an appropriate technology and signal processing method for a specific application. The strengths and limitations of the different technologies are yet to be clarified. Second, there are inconsistent views on the maximum measurement distance and anti-interference capability of these technologies, which have hindered the acceptance of the technologies in applications. To date, these technologies (i.e., GNSS, microwave radars, laser-based methods, and computer vision methods) have not been reviewed from the perspective of electromagnetic waves.

Therefore, there is a need to establish a holistic understanding of the links and differences of these technologies. This review aims to: (1) clarify the features and challenges of the technologies; (2) interpret the inconsistent viewpoints of the reviewed technologies; and (1) develop a decision tree model to facilitate the selection of appropriate technologies. To achieve these objectives, this paper starts with reviewing the measurement principles, data processing methods, and state-of-the-art applications of these technologies, and then discusses the features and selection of appropriate technologies. This review is expected to fill the knowledge gap at the interface between metrology and applications in civil structures, and promote technology development.

The remainder of this article is organized as follows. Section 2 provides an overview of the fundamental knowledge of the technologies to help civil engineers follow the review. Section 3 introduces the data processing techniques for the reviewed technologies. Section 4 reviews the performance, applications of these methods, and compatibility with autonomous platforms. Section 5 discusses the strengths, limitations, and some inconsistent statements of the methods to help engineers choose suitable methods for intended applications. Section 6 summarizes the main conclusions and research prospects.

2. Overview and measurement principles

2.1. Overview

According to the wavelength, EM waves can be categorized into radio waves, microwaves, infrared waves, visible light, ultraviolet waves, X-rays, and gamma rays, as shown in Fig. 1 [32]. Propagation of EM waves involves reflection, refraction, and scattering, interference with other EM waves. The frequency range of radio waves is 30 Hz to 300 GHz, which is widely used in telecommunication, navigation systems, and distance measurement. Microwave radar uses EM waves ranging from 1 GHz to 100 GHz.

Fig. 2 categorizes the four families of technologies into point-to-point methods and point-to-surface methods. The point-to-point methods measure the distance of one or a limited number of points [35,62]. The point-to-surface methods measure the distances of a surface or a large number of points of a surface [83,157,158]. Depending on whether the transmitter and receiver are positioned at the same location, these technologies can be categorized into transceiver separated methods and transceiver integrated methods. The vision-based methods are point-to-surface methods with transceiver separated, because the vision-based methods use a camera to measure surfaces rather than single points and the camera collects the light signal reflected by the monitored objects and does not require a light source in the camera. When the point-to-point methods are used, it is difficult to obtain the distances of a surface or numerous points on a surface. However, when the point-to-surface methods are used, usually the distance of a single point can be obtained.

2.2. Point-to-point distance measurement

Point-to-point methods use EM waves (e.g., radio wave, microwave, and light wave) as carrier waves to modulate signals and measure the distance between two points [33]. The distance can be obtained by two methods: pulse-based method and phase-based method, as shown in Fig. 3.

Fig. 3(a) illustrates the pulse-based method, which determines the distance between the transmitter and receiver by measuring the transmitted and received pulses. Once the time of flight of the pulse is determined, the distance can be calculated using Eq. (1) [33]:

$$d = \frac{c}{nk}\Delta t \tag{1}$$

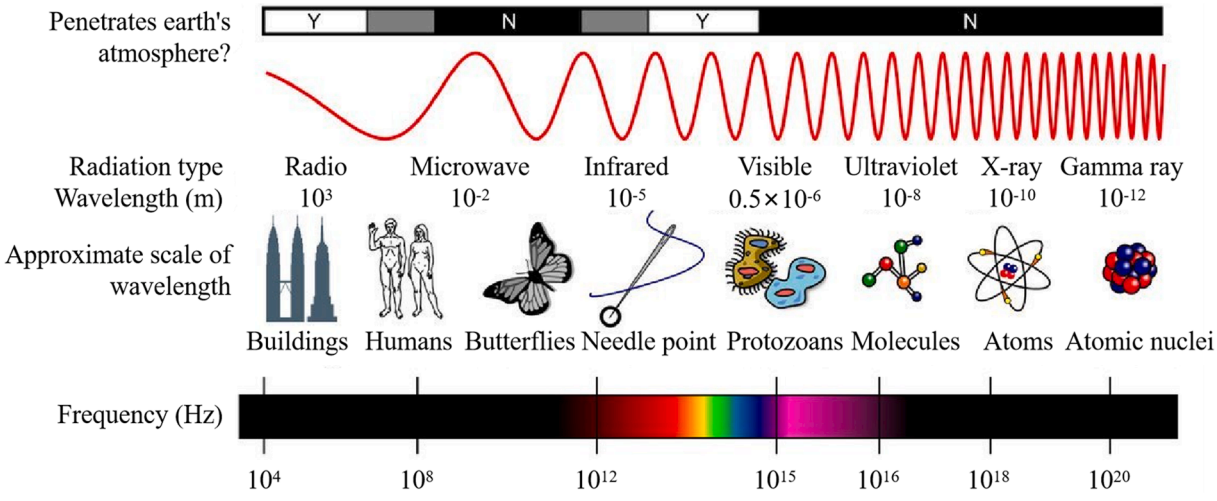

Fig. 1. Depiction of the spectra and the corresponding scale of different EM waves [32].

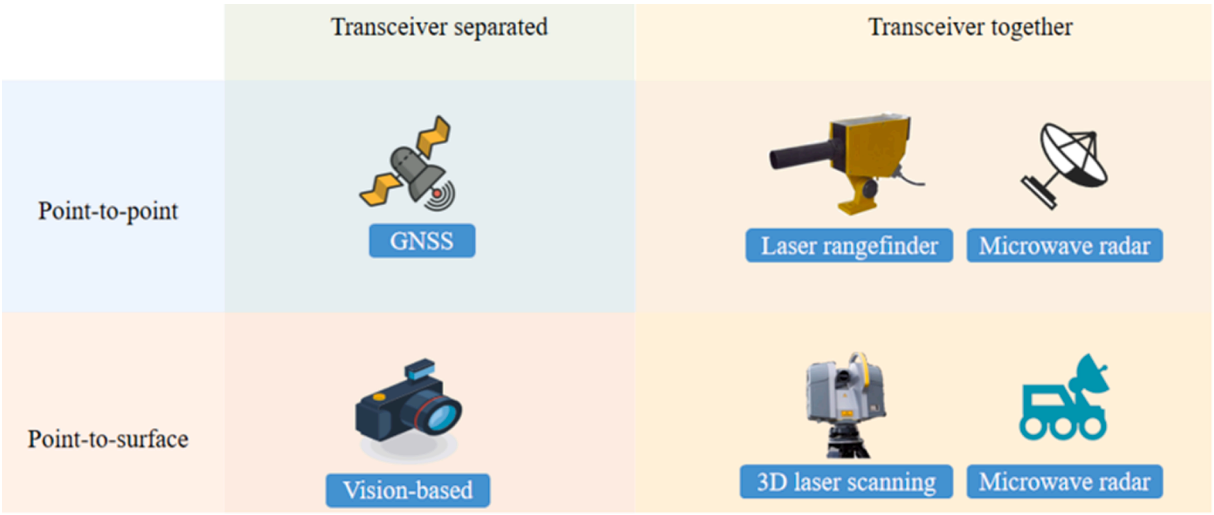

Fig. 2. Categories of the distance measurement technologies based on EM waves.

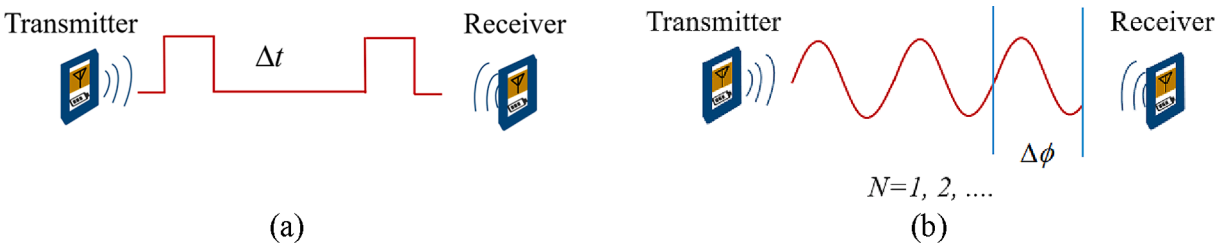

Fig. 3. Schematic of point-to-point measurement methods: (a) pulse-based; and (b) phase-based.

where c is the speed of EM wave in vacuum; Δt is the time of flight; n is the refractive index of the propagation medium; k is a coefficient of scenario: (1) $k = 1$, if the transmitter and receiver are at two different locations (single trip); and (2) $k = 2$, if the transmitter and receiver are at the same point (round trip).

Fig. 3(b) illustrates the phase-based method, which determines the distance by measuring the phase difference of EM waves between two points. With the phase change, the distance can be calculated using Eq. (2) [33]:

$$d = \frac{\lambda}{k}\left(N + \frac{\Delta\varphi}{2\pi}\right) \tag{2}$$

where N is the integer number of the wavelength when electromagnetic wave propagates between transmitter and receiver; $\Delta\varphi$ is the phase change, which denotes the fractional part of the wavelength; λ is the wavelength.

According to the above principles, the spatial resolution and the measurement accuracy of the pulse-based method mainly depend on the measurement of the time of flight, and the spatial resolution and the measurement accuracy of the phase-based methods mainly depend on the measurement of the phase change. To achieve a high spatial resolution, the pulse-based method needs a narrow pulse width (a small Δt), and the phase-based method needs a high resolution of the phase change (a small $\Delta\varphi$). In general, the phase-based methods have achieved higher spatial resolutions (millimeter order) than the pulse-based methods, because it is more challenging to achieve a high spatial resolution with a narrow pulse width. According to Eq. (1), a millimeter resolution needs a pulse width at a picosecond level, which requires costly devices and sophisticated signal processing. However, cost-effective devices can be used to achieve a high spatial resolution using phase-based methods. Similar to the spatial resolution, the pulse-based method needs more costly hardware than the phase-based method to achieve a high measurement accuracy. Besides, the measurement accuracy is also affected by noises [25]. Further discussions on the accuracy and resolution are included in Section 5.

Representative methods based on the point-to-point principles include GNSS and microwave radar methods. GNSS is a general term of satellite navigation systems, such as the global positioning systems (GPS), global navigation satellite systems (GLONASS), BeiDou, Galileo, etc. [33]. The distance between a satellite and a receiver is determined by the time or phase difference [34]. Examples of microwave radar techniques include frequency modulated continuous wave radar, stepped frequency continuous wave radar, interferometric radar, and pulse ultra-wideband radar. The radar system transmits microwaves to the target and receives the signals reflected by the target. The distance is determined by measuring the time of flight or the phase change of the reflected signal and the transmitted signal [35,36].

2.3. Point-to-surface distance measurement

2.3.1. Three-dimensional point cloud

Based on the principles in Section 2.2, lasers have been used to measure distance because lasers have multiple advantages, such as straight-line propagation, good monochrome, strong directionality, and narrow beam. Traditionally, lasers were used for point-to-point measurement. Recently, laser scanners have been developed to measure distance for many points by scanning a surface. The measured distance of a surface can be used to generate 3D point clouds, which are then used to generate 3D structural models, as illustrated in Fig. 4. A laser scanner is used to scan the surfaces of a structure. Point clouds are generated and used to reconstruct the 3D digital model of the structure. Structural deformation can be monitored by tracking changes of the point cloud using sophisticated signal processing techniques, which are discussed in Section 3. Point clouds can be obtained by not only laser scanners but

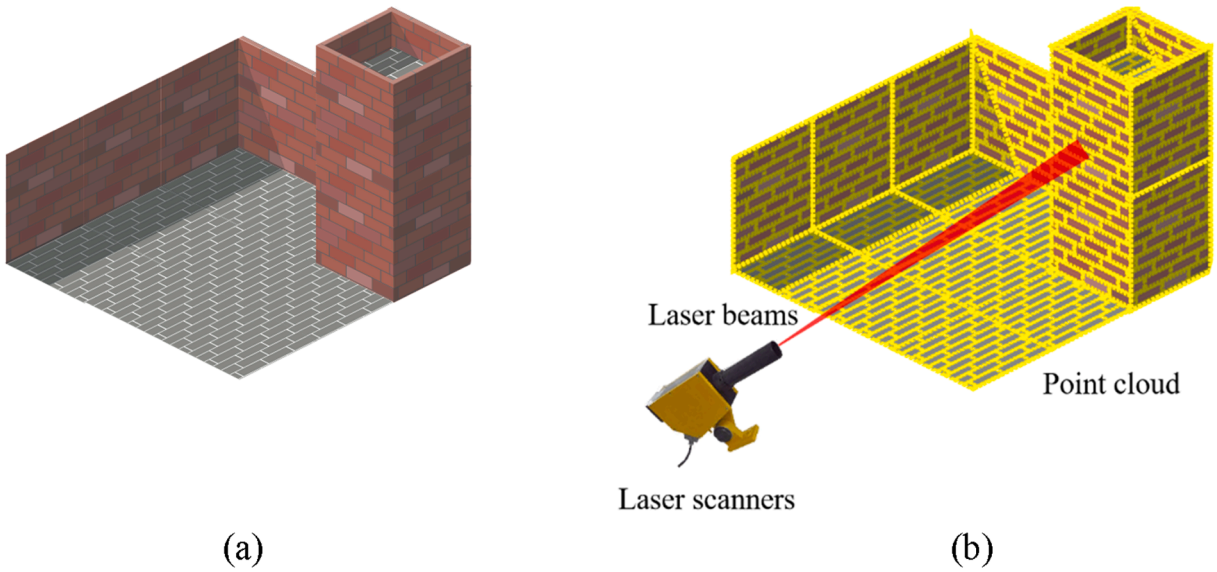

Fig. 4. The surface of a building can be scanned to form a 3D point cloud: (a) a sketch of the building, and (b) the point cloud measured a laser scanner for the building.

also other devices which are capable of multi-channel geodetic ranging, such as RGB-D depth cameras [37], binocular cameras [38], and interferometric synthetic aperture radar [39]. In addition to the distance measurement, point cloud data could incorporate other information (e.g., color) for measurement of temperature [40], and chemistry [41].

2.3.2. *Computer vision*

Based on the number of cameras used for the measurement [42,43], computer vision-based measurement methods can be classified into two categories: (1) Category 1: monocular camera; and (2) Category 2: binocular cameras, as depicted in Fig. 5.

The measurement principle of monocular camera is based on aperture imaging, as shown in Fig. 5(a). The distance between the camera and the target can be calculated [42]:

$$d = \frac{w}{p} f \tag{3}$$

where w is the real width of an object; p is the pixel width of the object on the photo; and f is the focal length of the camera. The measurement of distance has been realized using moved camera [44], structured light [45], and other referenced-object methods [46].

The principle of binocular camera for distance measurement is similar to the working principle of human eyes [47]. The distance can be calculated using similar triangles and disparity when two cameras are placed in parallel, as shown in Fig. 5(b). The formula for calculation of distance is shown in Eq. (4) [43]:

$$d = \frac{fb}{x_l - x_r} \tag{4}$$

where d is the distance to be measured; b is the baseline distance between two cameras; f is the focal length; x_l and x_r are the coordinates of the two images from the optical axis [43].

Based on the above principles, the cameras of phones have been used to measure displacement [48,49]. In addition, advanced depth cameras (RGB-D) have been used [50,51]. Measurement of distance based on

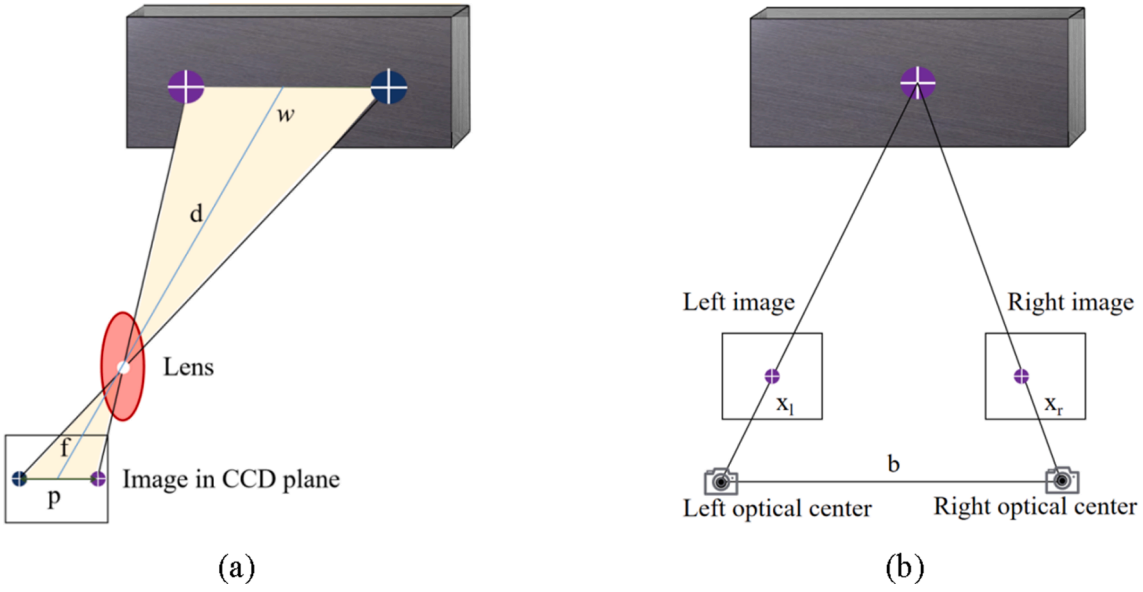

Fig. 5. Vision-based measurement of distance: (a) monocular method, and (b) binocular method.

computer vision methods demands tracking of "target" on the structure. The "target" can be artificial (e.g., a preinstalled marker or panel with special patterns) or a structural feature (e.g., bolts or holes) [52]. The target tracking algorithm is introduced in Section 3.

3. Data processing methods

With the data measured from the sensors of the reviewed technologies, data processing is performed to analyze the distance and minimize errors. The data processing methods for the reviewed technologies are reviewed.

3.1. GNSS

In the applications of GNSS methods, errors are generated in the propagation of EM waves. The typical errors include the ephemeris error, ionospheric error, tropospheric errors, multipath error, and measurement noise [53]. Table 1 lists some representative studies on improving the measurement accuracy through signal processing. Different methods have been proposed to mitigate different errors. For instance, the ephemeris error, ionospheric error, and tropospheric errors were minimized by the differential technology utilizing reference stations with known 3D coordinates [53]. The measurement of two receivers that track the same satellite contains similar deviations, which were used to minimize the errors [54,155]. The calculation of the distance depends on a subtraction operation. For example, real-time kinematics (RTK) positioning system is a differential GNSS technology which achieved an accuracy at millimeter-level (2–3 mm) for displacement monitoring [55,56]. The multipath error and measurement noises were reduced by fast Fourier transform [53], sidereal filtering [57], wavelet transform [58,59], principal component analysis [60], empirical mode decomposition [61], Chebyshev filtering [62], moving average filtering [63], and neural networks [64,65]. For instance, Quan et al. [65] proposed a convolutional neural network that detected about 80% multipath errors and improved the accuracy by up to 30%.

Table 1
Methods for reducing errors in GNSS distance measurement.

Source	Algorithm	Problem	Time or frequency	Verification method
[53]	Fast Fourier transform, moving average filtering	Data extraction	Both	Field test
[57]	Sidereal filtering, wavelet transform, and double reference shift strategy	Mitigating multipath error	Both	Laboratory test
[58]	Wavelet packet filtering	Mitigating multipath error	Both	Laboratory and field tests
[59,60,66]	Wavelet transform and principal component analysis	Noise reduction and data extraction	Both	Field test
[67]	Multi-filtering, wavelet transform, and Monte Carlo simulation	Noise reduction and data extraction	Both	Field test
[61]	Empirical mode decomposition and Chebyshev filtering	Noise reduction and data extraction	Frequency	Laboratory and field tests
[62]	Spectral analysis and Chebyshev filtering	Mitigating multipath error	Frequency	Laboratory and field tests
[63]	Moving average filtering	Noise reduction	Both	Field test
[64]	Neural network	Noise reduction	Both	Field test
[65]	Neural network	Mitigating multipath error	Both	Laboratory test
[68]	Differential GNSS and cubic spline fitting	Eliminating ephemeris error, ionospheric error, and tropospheric error	Both	Field test
[69]	Differential GNSS	Noise reduction	Both	Field test
[56]	Differential GNSS	Noise reduction	Both	Laboratory and field tests
[55]	Differential GNSS and multi-constellation	Noise reduction and data extraction	Both	Laboratory and field tests
[70]	Multi-constellation	Noise reduction	Both	Field test
[71]	Fusion of accelerometer	Accuracy and sampling rate improvement	Both	Laboratory and field tests

Multi-constellation has been proven effective in improving the measurement accuracy [53,55,70]. A receiver with the multi-constellation ability can obtain signals from multiple constellations (e.g., GPS and BeiDou) rather than a single type of constellation. For GNSS, in order to locate a receiver on the earth, the receiver must receive signals from at least four satellites at the same time [156]. The data from different constellations can be compared to determine the distance [157]. Xi et al. [70] integrated GPS, BeiDou, and GLONASS to measure the deformation of the Baishazhou Yangtze River Bridge in Wuhan, China. The accuracy was as fine as 1.8 mm for a single GNSS system, 1.1 mm for the use of two GNSS systems, and 1.0 mm for the combination of GPS, BDS, and GLONASS systems. In addition, GNSS can be integrated with acceleration data and Kalman filter for improving the accuracy and sampling frequency of dynamic displacements [71]. For example, Kim et al. [71] proposed a Kalman filter for fusion of bridge displacements measured from a GPS and accelerations measured from accelerometers. The initial measurement of displacements had a root mean square error (RMSE) of 21.63 mm, and a sampling frequency of 20 Hz. After the Kalman filter was applied, the RMSE of displacements was reduced to 1.55 mm (by 93%), and the sampling frequency was increased to 100 Hz (by 400%).

3.2. Microwave radar

Compared with GNSS, microwave radar is an active sensing technology, which emits microwaves to objects and receives the reflected waves [72]. Based on the transmitting wave, the mainstream microwave radar methods can be classified into frequency modulated continuous wave (FMCW) radar and stepped frequency continuous wave (SFCW) radar [75].

Regarding FMCW radars, the transmitter sends a linear frequency signal [76,77]. The main challenge of signal processing is that the accuracy is affected by the slope and linearity of the frequency shift. To address the challenge, algorithms based on phase evaluation have been developed. Fig. 6 depicts a representative procedure for phase evaluation using an intermediate frequency estimation algorithm to determine the distance using echo signals [72,73]. First, the algorithm uses a windowing function to select a finite number of intermediate frequency signals in time domain, and reduce frequency bias by increasing the target peak width [74]. Second, zero-padding is applied to improve the resolution in frequency domain. Third, the Fourier transform is performed to convert the intermediate frequency signal from time to frequency domain [72]. Then, peak detection is performed to determine the intermediate frequency. Finally, interpolation is conducted to improve the accuracy [72,73]. With this method, Piotrowsky et al. [72] achieved a high accuracy (5 μm) for measuring distance with an operation distance of 5.2 m.

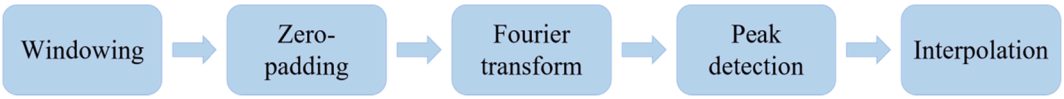

Fig. 6. Flowchart of signal processing procedure for measuring distance with an FMCW radar.

Regarding SFCW radars [78,79], the signal processing methods are similar to that of the FMCW radar method. The main difference is that the stepped frequency waveform contains a burst of monochromatic pulses with stepped-increasing frequency rather than a continuously increasing frequency [80]. The advantage of the SFCW radar is that the defects of the received signals for frequency identification can be compensated through data processing [81]. Based on SFCW signal modulation, Melo et al. [78] designed a radar to monitor structural displacement and achieved an accuracy finer than 0.2 mm for distances up to 400 m.

In addition to improving the accuracy, research has been conducted to enable imaging of structures. Imaging techniques based on microwave radars are emerging in remote sensing of structures and geological disasters, such as subsidence [82]. The representative imaging techniques include synthetic aperture radar [82], differential synthetic aperture radar interferometry [83], and pulse ultra-wideband radar [84]. The radar continuously transmits signals to the target structure, and uses the received signals to generate images of the structure, as illustrated in Fig. 7.

3.3. Laser scanning

Fig. 8 shows an application of a laser scanner for measuring the deformation of a tunnel [85]. After the point cloud data were obtained, data processing was performed in four steps: (1) Point cloud extraction was performed to separate areas or curves of the most interest. Regarding the tunnel in Fig. 8, the laser scanner was used to assess the cross section. (2) Errors in the point cloud data were reduced. A filter based on discrete wavelet transformation was adopted to reduce noises due to the presence of power lines on the tunnel lining. (3) Curve fitting was performed using an elliptical curve to reconstruct the 3D model and reduce the number of elements in the point cloud. Free-form curves were applied to describe the shapes of arch structure [86,87] and tunnel cross section [85,88], such as B-spline curve [86,88] and polynomial curve [87,89]. (4) Displacement was calculated based on the fitted curves in different epochs.

Laser scanning methods feature remote sensing and high acquisition efficiency, as well as the following limitations: (1) The acquisition of point cloud requires intensive efforts for planning and preparation. (2) Laser scanning devices are costly and need skilled engineers. (3) Advanced data storage and processing systems are needed to store and analyze a large amount of data collected from the laser scanner [90]. (4) The measurement accuracy depends on many factors, such as the details of the structure, the density of the point could, and various factors of noises.

3.4. Computer vision

The data processing algorithm for vision-based structural displacement measurement usually consists of four main steps [91,92]: camera calibration, feature extraction, target tracking, and displacement calculation, as shown in Fig. 9.

Features are unique characteristics for target tracking. Extracting robust features is the basis of target tracking and affects the accuracy [93–98]. In most applications, artificial targets are mounted on the structure, such as a concentric circle [94,95] and chessboard [96]. Fig. 10 shows representative types of targets. The brightness threshold is used to detect the edges, and the centroid coordinates are calculated to track the displacement of the targets. He et al. [94] proposed a six-layer concentric circle image with a size of 767 × 767 pixels, and optimized the number of circles and the size. Overall, it is time-consuming and costly to deploy artificial targets on site. Therefore, a variety of target-free methods that utilize features of the object structures have been proposed, as shown in Fig. 10(c) to (f).

Regarding displacement measurement for bridges, the optical turbulence errors were reduced by using an adaptive filter based on the statistical characteristics of optical turbulence errors. The accuracy has been improved from 0.845 mm to 0.0275 mm through two steps: (1) Step 1: primary displacement estimation; and (2) Step 2: application of the adaptive filter [100]. Further research is needed to explore the robustness of vision-based distance measurement in a harsh environment [101], such as dim light, background image disturbance, and partial template occlusion.

Data processing techniques have greatly improved the accuracy and reliability of vision-based methods [99]. Recently, the capabilities of data process and analysis have been enhanced by the advances in machine learning, such as artificial neural network and deep neural network [102], which help minimize human interventions and improve the measurement efficiency, accuracy, and reliability. More reviews on machine learning are included in Section 3.5.

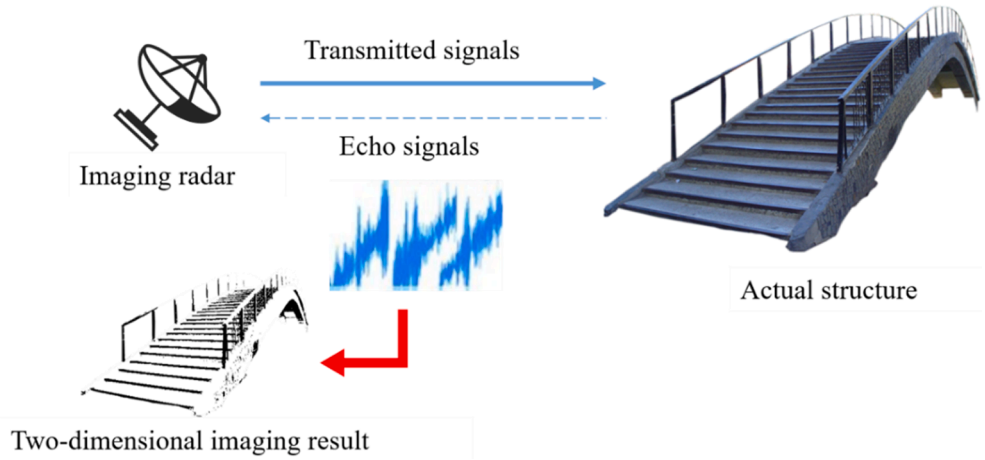

Fig. 7. Illustration of imaging a pedestrian bridge and its motion using a microwave radar.

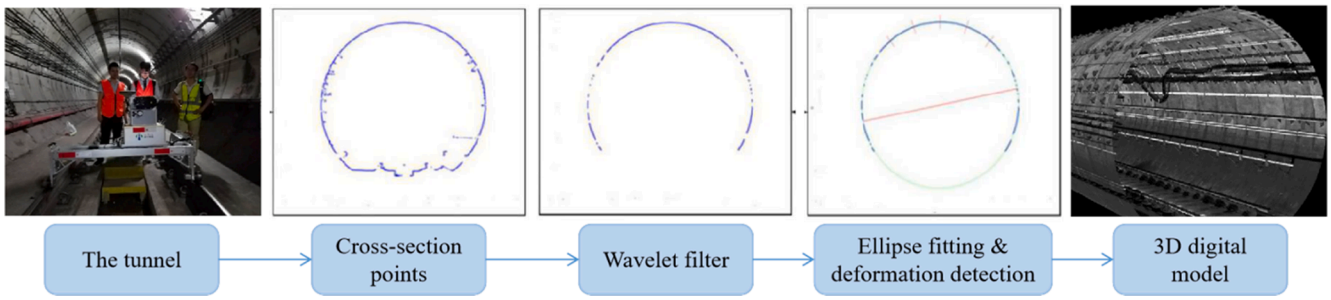

Fig. 8. The flowchart for deformation measurement and 3D reconstruction of a tunnel.

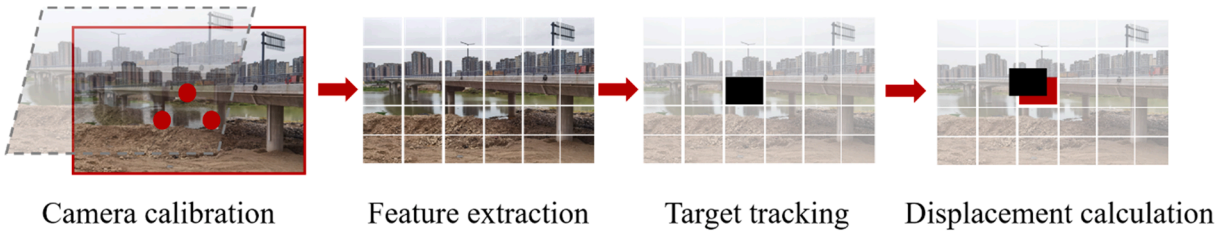

Fig. 9. Flowchart of a vision-based method for measuring displacement of a highway bridge.

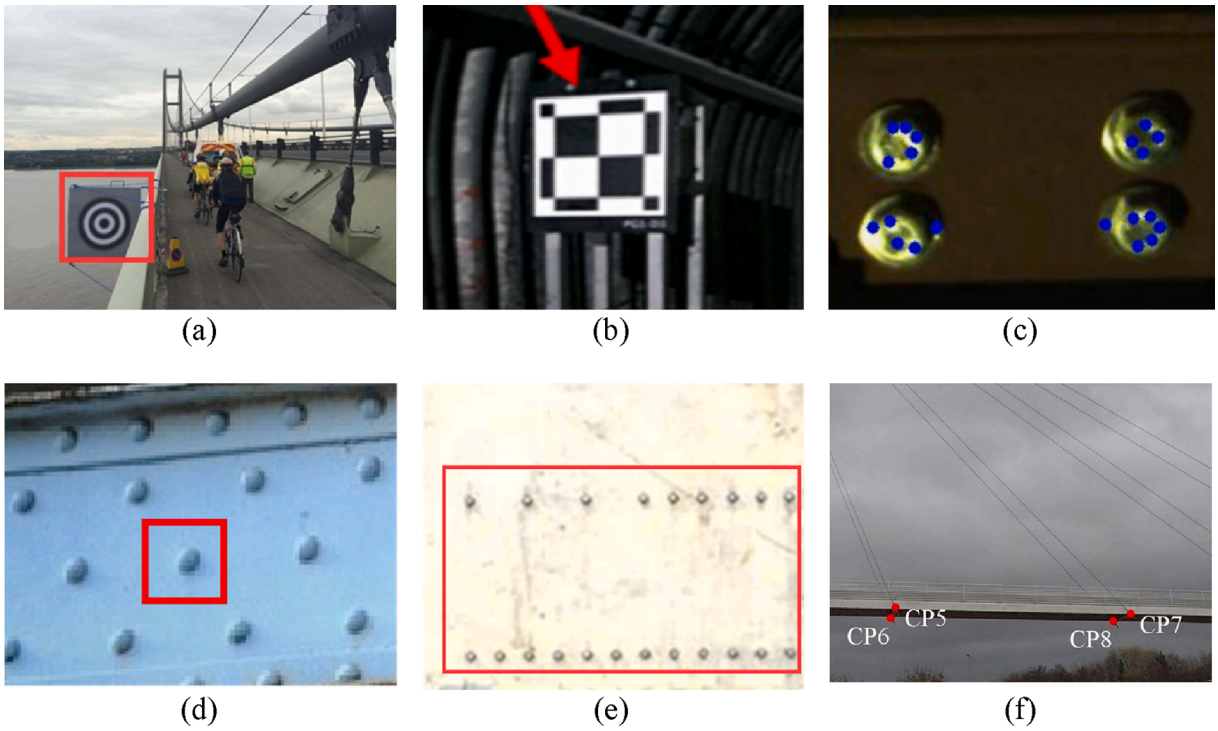

Fig. 10. Examples of targets used in vision-based structural health monitoring: (a) concentric circle [95], (b) chessboard [96], (c) Shi-Tomasi corner [92], (d) riveting point [98], (e) infrared targets [93], and (f) cable node [99]. Artificial targets are shown in (a) and (b), and natural targets are shown in the other figures.

3.5. Machine learning methods

Innovations have been made in incorporating machine learning in distance measurement. Traditional machine learning methods for distance measurement include support vector machines (SVM), empirical mode decomposition (EMD), maximum likelihood estimation (MLE), least square (LS), rank-based methods (RBM), and so on. Deep learning methods used for distance measurement are based on deep neural networks, such as artificial neural networks (ANN), convolutional neural network (CNN), mask regions with convolutional neural network (Mask R-CNN), long short-term memory (LSTM), extreme learning machine (ELM), and so on.

Table 2 lists representative research on machine learning methods which have shown advantages in different scenarios: (1) Reduce the noise of EM signals [64,65,103–105]. Kaloop et al. [64] used an ANN model to reduce the noise and multipath residuals of GPS signals. The standard deviation of the GPS signals was reduced by 3.5%, and the maximum displacement of the target was 1.17 mm. (2) Classify the causes of displacements [106–108]. Anantrasirichai et al. [106] proposed a CNN model which classified the causes of displacements based

Table 2
AI-enhanced algorithms applied in data processing.

Source	Year	Technology	Algorithm	Contribution
[64]	2014	GNSS	ANN	Proposed an ANN to reduce the receiver noise and multipath residuals of GPS signals
[65]	2018	GNSS	CNN	Proposed a CNN to detect multipath errors in measurement of distance
[104]	2017	GNSS	SVM and ELM	Proposed an ELM for the displacement of reservoir landslides with chaos characteristics
[105]	2020	GNSS	EMD and ELM	Used EMD and ELM to decompose the displacement of bridge and improve the prediction accuracy
[106]	2018	Microwave radar	CNN	Applied a CNN on interferograms of an interferometric synthetic aperture radar to detect volcanic deformation
[107]	2019	Microwave radar	CNN	Proposed a CNN on synthetically generated interferograms to detect deformation
[108]	2019	Microwave radar	CNN	Proposed a CNN to detect slow, sustained deformations using an interferometric synthetic aperture radar
[103]	2019	Laser scanning	SVM and MLE	Applied SVM and MLE to monitor the deformations of a building
[109]	2020	Laser scanning	RBM and LS	Proposed an RBM to reduce the RMSE of geometric modeling of a tunnel from 26.31 mm to 4.96 mm
[110]	2021	Laser scanning	ANN	Proposed an ANN and point clouds for calculating displacements of structures with an 85% success rate
[97]	2020	Vision-based	CNN	Proposed a CNN to determine displacements of a footbridge while eliminating artificial targes and human intervention
[111]	2020	Vision-based	Mask R-CNN	Proposed a Mask R-CNN to extract structural displacements from calibration objects
[112]	2020	Vision-based	CNN and LSTM	Applied CNN and LSTM to measure the vibrations of a structure

on a single radar interferogram. With the interferogram data for 12 days, high rates (1.8 m/year) of deformations were determined. (3) Improve the measurement accuracy and efficiency [103,109,110]. A nonparametric RBM model was proposed to reduce the RMSE of 3D reconstruction of a tunnel from 26.31 mm to 4.96 mm [109]. A CNN model was proposed to determine deformations of a footbridge while eliminating artificial targes and human intervention [97]. The measurable bridge displacement was finer than 2 mm, and the vibration frequency was 2.467 Hz, consistent with the results obtained from accelerometers.

Despite the advantages of the machine learning methods, multiple limitations have been identified from the existing studies: (1) A large dataset is needed to train and test the machine learning model. For instance, 30,249 interferograms were obtained and used to train the CNN model [106], and the training of the model took 38 h. When the size of dataset is small, the trained model cannot provide reasonable results of distance. Unfortunately, in many applications, there is insufficient data to train the model. (2) The generalization performance of the existing models is insufficient. Even if a machine learning model is trained using a large dataset, the model may not provide accurate results for different cases, which is a common issue for many machine learning models [113].

3.6. Relationship between signal processing algorithms

From the perspective of EM waves, the signal processing methods of the four technologies are related. Regarding the point-to-point methods, the measurement is subjected to errors caused by EM interference and variation of the propagation medium, and the errors can be reduced by spectrum analysis, such as wavelet transformation. An arbitrary EM wave can be expressed using a combination of sine functions determined through Fourier analysis of sinusoidal monochromatic waves. Regarding the point-to-surface methods, more attentions have been focused on locating the target and tracking its motion [3]. However, it is difficult to locate and track the target, due to unclear images and interference of lighting [3,48]. The errors can be analyzed and minimized using machine learning algorithms (e.g., convolutional neural network) [3,48].

Fig. 11 compares the capabilities of the different families of post-processing methods. Traditional displacement sensors mainly measure time-domain signals, while microwave radar, laser scanning, and vision-based technologies could generate images. The differential technology and multi-constellation technology are based on subtraction and comparison operations, respectively. Spectrum analysis is based on Fourier transform, which is more complex than the subtraction and comparison operations. Machine learning involves more complex algorithms than Fourier transform. Therefore, the complexity of these processing methods can be compared, as illustrated in Fig. 11. New data processing methods have been presented to utilize machine learning methods to improve the efficiency, accuracy, and reliability.

4. Performance in distance measurement

4.1. Representative applications

The reviewed technologies have been applied to condition assessment of various structures, including bridges [114,115], buildings [118,123], tunnels [85], dams [133], slopes [116], towers [124], and wind turbines [158]. In real-life applications, the deployment of sensors and setup of the instruments are critical to ensure a desired performance. To review the sensor deployment and setup of the instruments, some representative examples of the reviewed technologies are displayed in Fig. 12. Typically, a GNSS system uses one of the four modes: real-time kinematic (RTK), post-processing kinematic (PPK), network-based real-time kinematic (NRTK), and kinematic precise point positioning (PPP) [30]. Among the four modes, RTK and PPK require a fixed base station near the monitored structure. The difference between RTK and PPK is that RTK supports real-time measurement but PPK does not support real-time measurement. The NRTK mode does not require a different base station, but uses a reference station that is continuously operated. In the kinematic PPP mode, the distance is calculated using the carrier phase and independent on the ground base station.

In Fig. 12(a), a GPS receiver was installed in the middle of the main span of a bridge to monitor the vibration of the bridge under operation loads [114]. Another receiver was fixed to the ground as a reference. The distance between the GPS receiver and the reference was about 300 m. By analyzing the data collected for 60 s at the sampling frequency of 100 Hz, the dynamic characteristics of the bridge were obtained. The maximum mid-span deflection was 8 mm, and the vibration frequency was up to 8 Hz, consistent with the results from displacement sensors and accelerometers, respectively.

Fig. 12(b) shows a microwave radar which was supported by a tripod underneath a bridge to monitor the vibration of a bridge girder [115]. Microwaves were emitted by the radar, and the signals reflected from bridge girder were received by the same device with a sampling frequency of 30 Hz. The distance between the radar and the girder was 4.3 m. The fundamental natural frequency of the bridge was measured to be 9.4 Hz, which agrees well with the measurement results from accelerometers installed on the bridge.

Fig. 12(c) shows a high-speed phase laser scanner with a 360-degree

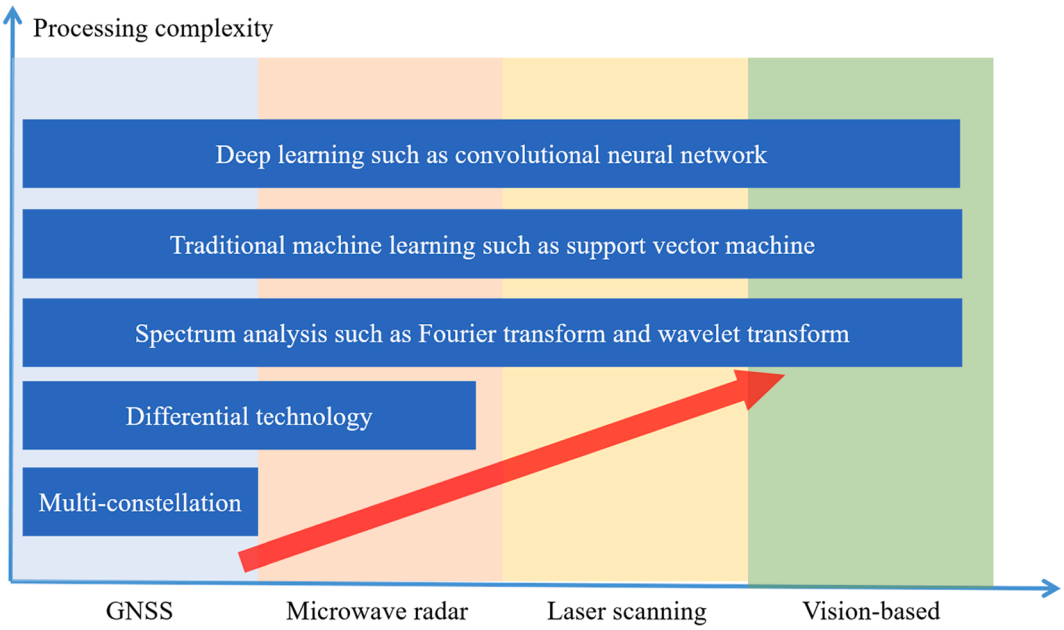

Fig. 11. Data processing methods of the reviewed technologies. The red arrow indicates that the processing complexity of the method increases. (For interpretation of the references to color in this figure legend, the reader is referred to the web version of this article.)

field of vision. The laser scanner was carried by a trolley and used to measure the deformation of a tunnel. The scanning speed can be more than 1 million points per second, and the maximum scan speed was 200 contours per second. The laser scanner was used to obtain more than 2.4 billion points on 396,762 cross sections within 16 min [85]. The distance between the laser scanner and the tunnel was about 3 m. The measurement accuracy was 1.5 mm. The repeatability of the global and local deformation measurements was 0.5 mm and 0.9 mm, respectively. The accuracy satisfied the requirement of deformation measurement of tunnels, and the efficiency was higher than the use of total station which took 10 min to measure one cross section and demand targets installed on the tunnel lining [85].

Fig. 12(d) shows a 109-m cable-stayed bridge monitored using a vision-based method [99]. A camera (model: GoPro Hero 4) was mounted on a tripod at the central reservation of a carriageway. The distance between the camera and the measuring point on the bridge was 55.3 m. The sampling frequency was 30 Hz. The image size was 1920 × 1080 pixels. The test was continued for 4 h. The bridge vibration was measured under a cloudy weather. With certain pedestrian loads, the maximum deformation of the bridge was 72.58 mm. The vibration frequency of a stayed cable was 2.08 Hz, consistent with the measurement results from accelerometers.

4.2. Performance metrics

Table 3 lists representative performance metrics of the reviewed technologies in recent applications. The investigated performance metrics include the measurement accuracy, sampling frequency, operation distance, and monitoring time. The monitoring time describes whether the technology is used for long-term or short-term monitoring.

Regarding the GNSS method, the accuracy ranges from sub-millimeter to tens of millimeters; the sampling frequency is from 1 Hz to 100 Hz; the operation distance is large because satellites are used for measurement, and the method can be used for both long-term and short-term measurements. Regarding microwave radars, the accuracy ranges from sub-millimeter to a few millimeters; the sampling frequency is up to 1000 Hz; the operation distance has reached 145 m; the method was used for short-term measurement in the prior studies. Regarding the laser scanning method, the accuracy ranges from sub-millimeter to a couple of millimeters; the sampling frequency is up to 200 Hz; the operation distance has reached 2500 m; the method was used for both long-term and short-term measurements. Regarding the vision-based method, the accuracy is finer than a millimeter; the sampling frequency is up to 60 Hz; the operation distance has reached 2080 m; the method was used for short-term and long-term measurement in the prior studies.

Fig. 13 compares the performance metrics of the reviewed technologies, including the measurement accuracy, frequency, operation distance, and monitoring time. These performance metrics are dependent on the hardware and data processing programs. The highest accuracy of each technology has reached millimeter or even sub-millimeter order, which is adequate for structural health monitoring of engineering structures in many cases. Regarding the frequency, the reviewed technologies have demonstrated the capability of measurement at frequencies higher than 100 Hz. In measurement of vibrations, the sampling frequency needs to be at least twice the frequency that needs to be measured according to the Nyquist Theorem [114]. The interested frequency of many civil engineering structures is up to 30 Hz [115]. Therefore, the desired sampling frequency should reach 60 Hz. In this sense, the reviewed technologies are capable of dynamic measurement. The operation distances of the reviewed technologies have been longer than 1000 m, enabling remote measurement. Although microwave radars were mainly used for short-term measurement, they are available for long-term measurement according to their working principles, but further research is needed to evaluate their long-term performance.

4.3. Autonomous platforms

A variety of autonomous platforms have been employed to promote the operation of the reviewed technologies for condition assessment. Representative autonomous platforms include UAV [131], manned or unmanned aircrafts [135,136], and satellite-based platforms [22,23]. The autonomous platforms carry sensors and/or instruments to measure distance, thus, significantly improving the mobility and efficiency of measurement. Fig. 14 illustrates the vision of using autonomous platforms [137].

UAVs have been used to carry microwave radar [38], laser scanner [32], and cameras [131,138] to approach difficult-to-reach regions and

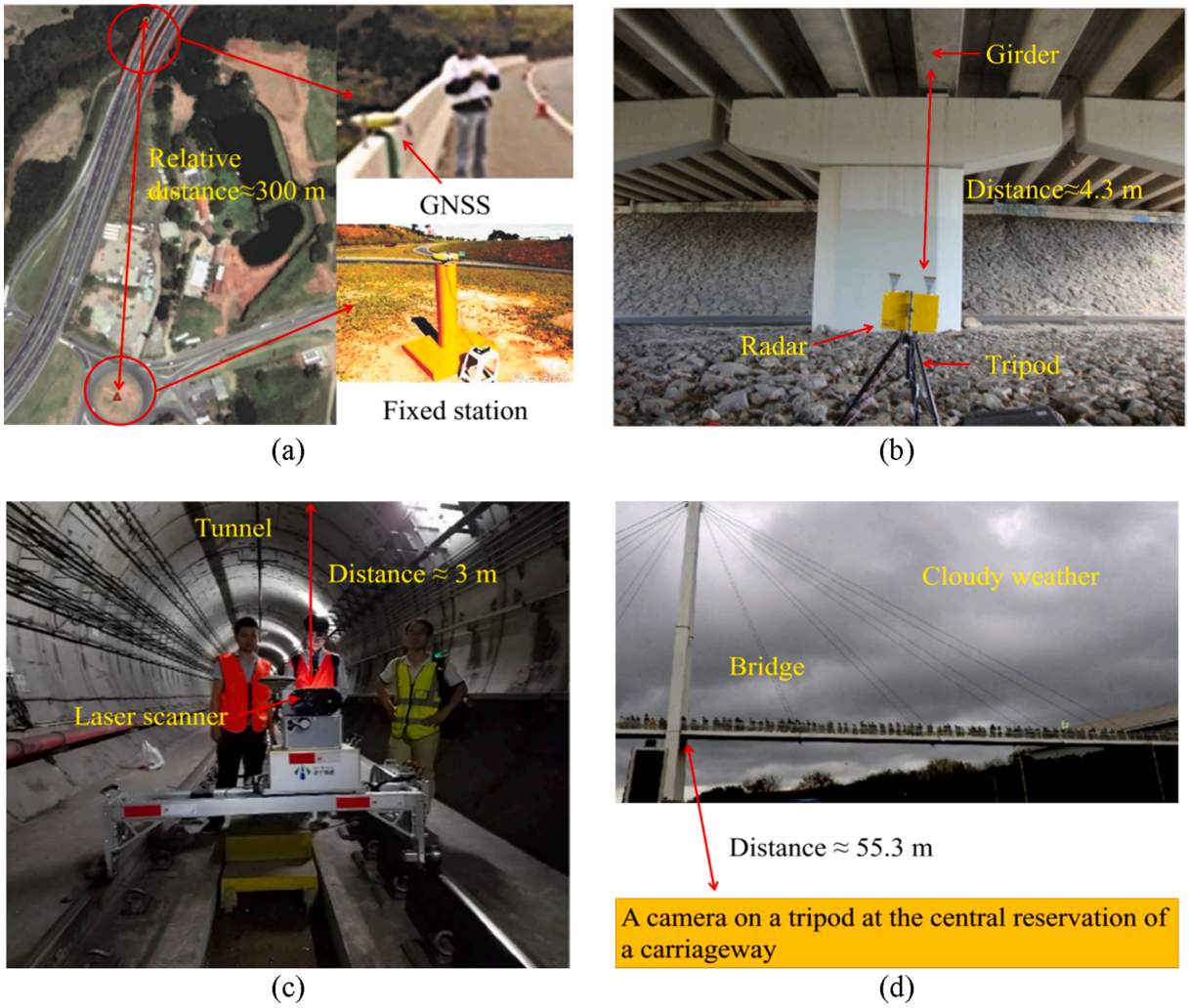

Fig. 12. Representative applications of: (a) GNSS-based method [114], (b) radar-based method [115], (c) laser scanner-based method [85], and (d) vision-based method [99].

measure displacements and vibrations of bridges [131,138], buildings [139], and towers [140]. As the size and weight of laser scanners are reduced [141,142], laser scanners can be installed on an UAV to scan a bridge for measuring bridge vibrations. For example, the displacement of a moving target could be measured using an UAV at various distances (4 m to 7 m) away from the bridge, and the peak error and RMSE were <2 mm [32]. A commercial UAV was used to monitor a railway bridge in real time with a high-resolution camera [131]. The UAV was 4.6 m away from the bridge, and the RMSE was 2.14 mm. In addition, UAV has been used to capture videos which were used to analyze the vibration of a suspension bridge [138]. The camera installed on UAV had a resolution of 4,096 × 2,160 pixels and the sampling rate was set to 60 Hz.

The manned or unmanned aircraft can deploy microwave radar to conduct large area measurements [135,136]. The University of Kansas' Center for Remote Sensing of Ice Sheets deployed onboard manned or unmanned aircraft to carry microwave radar systems to continuously observe the Earth's cryosphere, including ice surface topography, ice thickness, and bedrock topography. With a compact FMCW radar system, operating from 2 GHz to 8 GHz, the seasonal snow depth between 0.3 m and 15 m was observed [136].

The satellite-based platforms have been employed for the GNSS technology [22,23], microwave radars [82,143], and laser-based method [144]. Microwave radars and laser-based methods have been incorporated into satellite-based platforms to assess the deformations of high-speed railways [143], monitor the deformations of bridges [39,82], dams [145], and buildings [145]. For example, a synthetic aperture radar on Envisat, which was the world's largest civilian Earth observation satellite, was used to monitor uneven settlement of the Beijing-Shanghai Railway and measured the settlement rate which was 24 mm per year [143].

The employment of autonomous platforms has shown many advantages: (1) Robots may have access to zones that are hard-to-access by human. This strength is particularly important in a harsh environment that is inappropriate for human, such as fire hazards and nuclear reactors. (2) Robots may have higher efficiency and lower cost because they can work continuously with no or limited downtime. (3) The satellite-based platforms offer the potential for all-time working capabilities without interference in routine operations. However, the use of satellites may involve high upfront costs, and the application of UAV-based platforms is often restricted by government [131].

5. Selection of appropriate technology

5.1. Inconsistent application performance statements

Currently, there are inconsistent viewpoints about the performance of these technologies. Regarding the measurement distance, on one hand, the reviewed technologies have been used for long-distance measurement. On the other hand, some studies reported that the accuracy of these technologies was compromised when the operation

Table 3
Representative applications and performance of the reviewed technologies.

Method	Structure	Accuracy (mm)	Sampling frequency (Hz)	Operation distance (m)	Monitoring time	Year	Source
GNSS	Bridge	<1	100	Space distance	Long	2019	[114]
	Slope	5.2	1		Long	2020	[116]
	Chimney	3	10		Long	2017	[117]
	Building	2	100		Long	2017	[118]
	Blade	20	5		Short	2013	[56]
	Others	0.62	10		Short	2020	[60]
Microwave radar	Bridge	–	30	4.3	Short	2016	[115]
	Bridge	–	100	612	Short	2020	[119]
	Bridge	–	66	240	Short	2020	[120]
	Bridge	<1	–	2.48	Short	2017	[121]
	Bridge	0.01	100	<20	Short	2019	[122]
	Building	0.01	78.8	34.5	Short	2013	[123]
	Tower	0.01	40	254	Short	2017	[124]
	Dam	<0.03	<0.01	1300	Short	2017	[125]
	Others	0.235	12	50	Short	2015	[36]
	Others	0.025	250	1.4	Short	2017	[25]
Laser scanning	Bridge	0.6	–	6.15	Long	2019	[126]
	Bridge	6	–	50	Short	2017	[127]
	Tunnel	1.5	200*	3	Short	2019	[85]
	Building	<2.5	–	15	Short	2017	[127]
	Retaining wall	<1	–	10	Short	2016	[128]
	Slope	–	–	2500	Short	2019	[129]
Vision-based	Bridge	<1	60	52	Short	2020	[97]
	Bridge	<0.5	–	<5	Short	2020	[130]
	Bridge	0.037	30	55.3	Short	2018	[99]
	Bridge	–	60	2080	Short	2020	[100]
	Bridge	2.14	24	4.6	Short	2018	[131]
	Bridge	1.1	1/60	20	Long	2020	[132]
	Dam	0.89	20	50	Short	2019	[133]
	Others	0.17	30	3	Short	2020	[134]
	Others	0.03	150	3	Short	2020	[100]

* Regarding laser-based method, the sampling frequency stands for the scanning frequency.

distance was increased. For example, a microwave radar achieved an accuracy of 0.235 mm when the operation distance was no more than 5 m [36]. A laser-based method achieved an accuracy of 0.082 mm when the operation distance was <20 m [128]. A vision-based system achieved an accuracy of 0.166 mm when the operation distance was <3 m [134]. Regarding the robustness to the environment, some researchers claimed that GNSS and microwave radar systems can work under extreme weather conditions [25,128], but other researchers reported that the measurement accuracy was compromised [35,100]. Table 4 lists the inconsistent opinions which hinder a suitable selection of these technologies.

The inconsistent opinions are caused by the different equipment characteristics, as well as the application scenarios. The performance of the technologies can be interpreted based on the working principles. The operation distance is related to the signal-to-noise ratio of the received signal, which is determined by the energy of the received signal and noises from environmental interference. The energy of the received signal is related to the transmitted power, frequency of EM wave, distance, and reflector property [146]. Regarding the transmitted power, frequency, and distance, the Friis Transmission Equation can describe the propagation of EM waves in the free space and can be used to calculate the received power (P_r) [147]:

$$P_r = \frac{P_t G_r G_t \lambda^2}{(4\pi d)^2} \tag{5}$$

$$\lambda = \frac{c}{f} \tag{6}$$

where P_t and P_r are the transmitted power and the received power, respectively; G_t and G_r are the transmitted and the received antenna gains, respectively; λ and f are the wavelength and frequency of the transmitted EM wave, respectively; d is the propagation distance of the EM wave; c is the propagation speed of EM waves. Based on Eqs. (5) and (6), if P_t is retained, P_r is inversely proportional to the distance d; if P_r and P_t are retained, λ is proportional to the distance d, which means f is inversely proportional to the distance d.

Regarding the reflector property, the transceiver-separated methods rely on the reflected EM wave, which has two effects: (1) The round-trip propagation distance is twice the single-trip measurement distance, and the received power is inversely proportional to the operation distance to the fourth power. (2) The surface of the target should reflect sufficient signal to the receiver. In microwave radar systems, radar cross-section (RCS) [148] is a measure of detectability of an object by radar, which denotes the EM signature of the object. For example, a microwave radar or laser scanner may need to use an artificial reflector with an adequate shape, orientation, and dielectric characteristics to enhance the reflectivity of targets [124].

The robustness to the environment also needs to consider the signal-to-noise ratio of the received signal. The propagation of EM waves is affected by atmospheric attenuation and ground reflection. Atmospheric attenuation describes the energy attenuation of EM waves during their propagation, which is associated with the frequency of the EM waves. When the frequency is <1 GHz, the attenuation is negligible. When the frequency is higher than 10 GHz, the attenuation is remarkable and increases with frequency. Presence of inhomogeneous media further aggravates the attenuation rate. In addition, ground reflection leads to multipath propagation of EM waves. Received signals are subjected to interference of direct and reflected waves. When the wavelength is reduced to centimeter-level, the ground reflection is close to diffuse reflection rather than mirror reflection, and the interference effect of the reflected wave can be ignored [146].

Based on the above discussions, the performance metrics in Table 4 can be interpreted: (1) The GNSS signals have less atmospheric attenuation because the frequencies of GNSS signals are lower than those of microwaves, lasers, and lights for vision-based systems. A GNSS system with a central frequency of 1.6 GHz (wavelength: 187.4 mm) is used for long-distance measurement [149]. The distance between a satellite and the earth is about 20,180 km to 25,800 km, and the transmitted power of

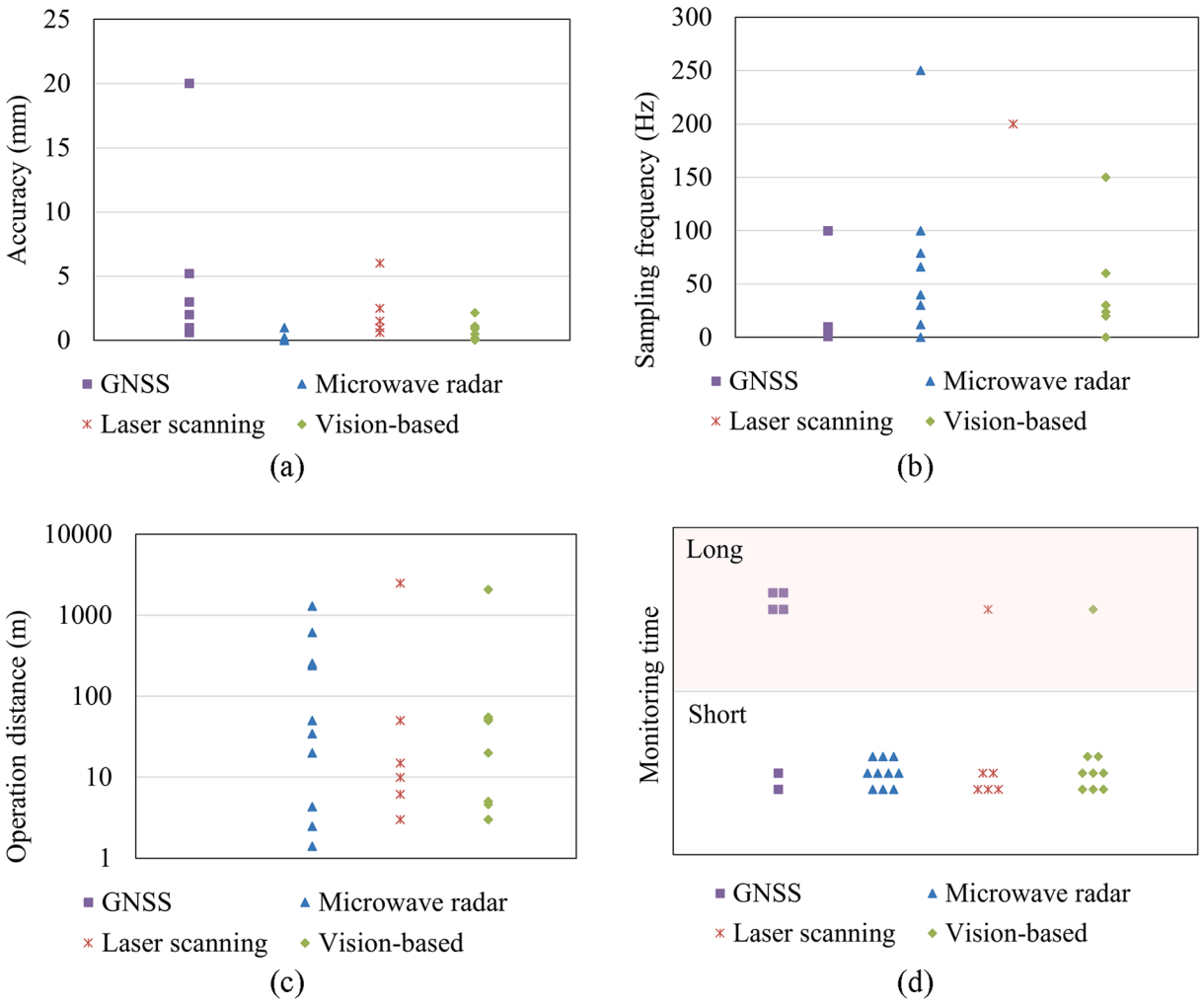

Fig. 13. Performance of the reviewed technologies: (a) accuracy, (b) frequency, (c) operation distance, and (d) monitor time. The distance of the GNSS technology is a space distance.

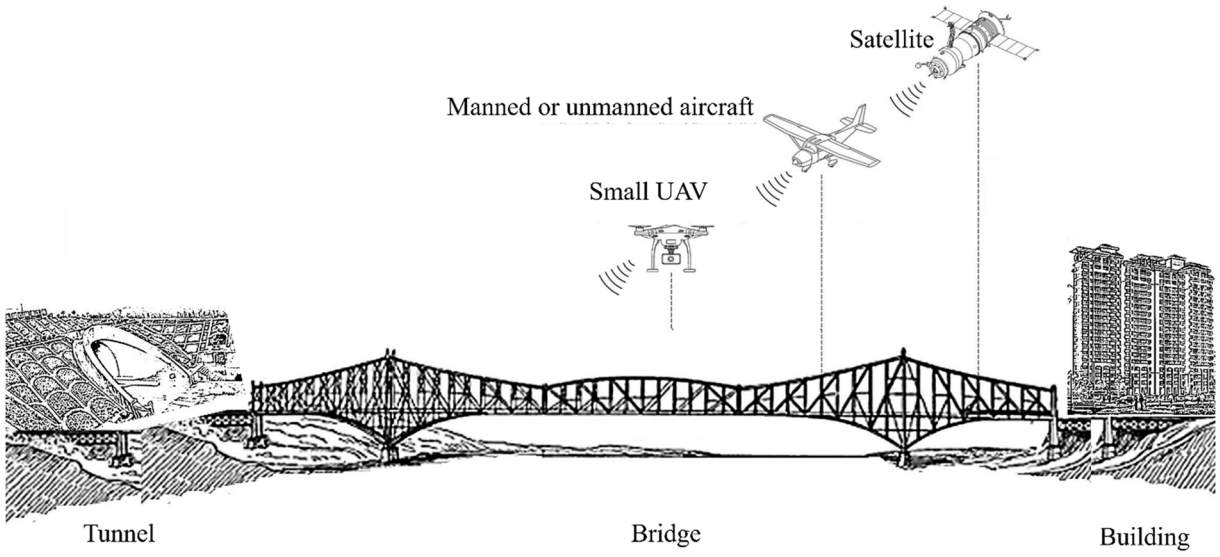

Fig. 14. Illustration of incorporating autonomous platforms into the reviewed technologies.

Table 4
Inconsistent application performance about the measurement distance and robustness.

Method	Long operation distance	Short operation distance	High robustness	Low robustness
GNSS	No limit on the earth [30]	None	Robust to environmental variables and weather [36]	Accuracy degraded in extreme weather [35]
Microwave radar	Anywhere on the earth [143]	≤5 m [36]	Robust to environmental variables and weather [25]	Susceptible to EM interference
Laser scanning	>1000 m [129]	≤20 m [128]	Robust to environmental variables and weather [128]	Sensitive to wind and ground motion [100]
Vision-based	2080 m [100]	3 m [134]	Robust to environmental variables and weather [99,100]	Accuracy degraded in extreme weather [35,36]

GPS satellite is 27 W (14.3 dBW) [150]. The transmitted antenna gain is 10 to 17. The received power is low but meets the minimum power requirement, which is 1.41×10^{-16} W (−158.5 dBW). (2) Regarding microwave radar systems, the range of the frequency is wider than the other technologies. Therefore, different systems in prior practices have shown different robustness to the environment. (3) When the laser-based and vision-based systems are placed near the object structure, the signal attenuation is small. Therefore, the receivers can receive signals with a higher signal-to-noise ratio and deliver high accuracy and robustness. Otherwise, when the laser-based and vision-based systems are far away from the structure, the measurement is sensitive to the environment.

5.2. Strengths and limitations of the technologies

Table 5 shows the strengths and limitations of the distance measurement technologies, in terms of the measurement accuracy, sampling frequency, operation distance, monitoring period, as well as the robustness to the environmental variables, computation cost in data processing, and capability in structural health monitoring. In general, the data processing methods of the point-to-point methods are relatively simple, but the point-to-surface methods provide more informative results. For example, point clouds of a structure can be used to generate 3D digital models of the structure, which are then used to greatly promote the management of the structure. In the field, point-to-surface measurement often requires skilled and well-trained engineers.

5.3. Decision tree

A decision tree is presented to facilitate the selection of appropriate technologies for specific applications, as shown in Fig. 15. The decision tree has a hierarchical structure with five layers which are designed to relate the specific application scenario and requirements to the performance of the technologies. The first layer of the tree is related to the type of measurement, e.g., point-to-point or point-to-surface. For example, measurement of the displacements at key sections of bridges or buildings can be performed by point-to-point measurement; and measurement of the curvature of a tunnel may need point-to-surface measurement. In the first layer, the reviewed technologies can be separated into two groups for further selection in the following layers. It should be noted that the proposed decision tree provides guidance for the selection of appropriate technologies based on the performance and features of the different technologies, but a comprehensive analysis is still needed in specific applications that involve other considerations that are not fully covered in this study.

Table 5
Strengths and limitations of selected distance measurement technologies.

Method	Strengths	Limitations
GNSS	• GNSS is applicable for large-scale structures (e.g., long-span bridges, high-rise buildings) • Applicable for long-term measurement	• The accuracy is sensitive to the obstacles • A high accuracy requires a reference GNSS near the target structure
Microwave radar	• Microwave is insensitive to the presence of obstacles (e.g., dust, rain, snow, etc.) • Microwave is robust to environmental variables (e.g., temperature, humidity) • Microwave radars can be used for long-distance measurement • Microwave radar actively emits energy, independent of sunlight, and works all day	• Subjected to EM interference • Artificial reflectors are often needed • The distance between adjacent target points should be at least 0.5 m • It is difficult to determine the direction of displacement
Laser scanning	• High accuracy and resolution • Point cloud data can be used to generate digital models of structures • No damage or additional mass to the object • No need of prior identification of the monitored points	• A large volume of data is collected • Detailed planning and preparation are needed to obtain point cloud [141] • The accuracy is sensitive to the operation distance and decreases rapidly with the increase of the operation distance
Vision-based method	• High accuracy and resolution • Measured data can be very informative (e.g., distance, temperature, chemistry, etc.) • Point cloud data can be generated by images or videos • Point cloud data can be used to generate digital models of structures	• The accuracy is sensitive to the operation distance, camera intrinsic parameters, and target tracking [151] • The accuracy is sensitive to light intensity, weather (e.g., rain), atmospheric refraction, and turbulence [99] • The light-of-sight condition is required • Intense computation is required

The presented decision tree only considers technical aspects. However, in real-life practices, economic aspects can be equally or more important, and, thus, they must be fully considered when multiple technologies can fulfill the technical requirements. For instance, when a point-to-surface method is needed but the lighting condition is not sufficient for vision-based methods, if the laser scanner equipment is not available, additional lighting equipment can be considered to enable the adoption of a more cost-effective vision-based method. In addition, integration of multiple technologies might improve the cost-effectiveness compared with a single technology [71,152]. For example, laser-based and vision-based methods were integrated to achieve cost-effective measurement of distance [130,153,154].

6. Conclusions and prospects

Effective distance measurement is significantly important in the construction, operation, and maintenance of civil infrastructure. This paper reviews four representative families of distance measurement methods based on EM waves, which include GNSS, microwave radar, laser-based, and vision-based methods. Based on this review, the following conclusions are drawn:

- The measurement accuracy of the reviewed technologies has reached a millimeter level. The GNSS systems can be operated to achieve a measurement frequency up to 100 Hz. Microwave radars can achieve a measurement frequency up to 1000 Hz, and the operation distance

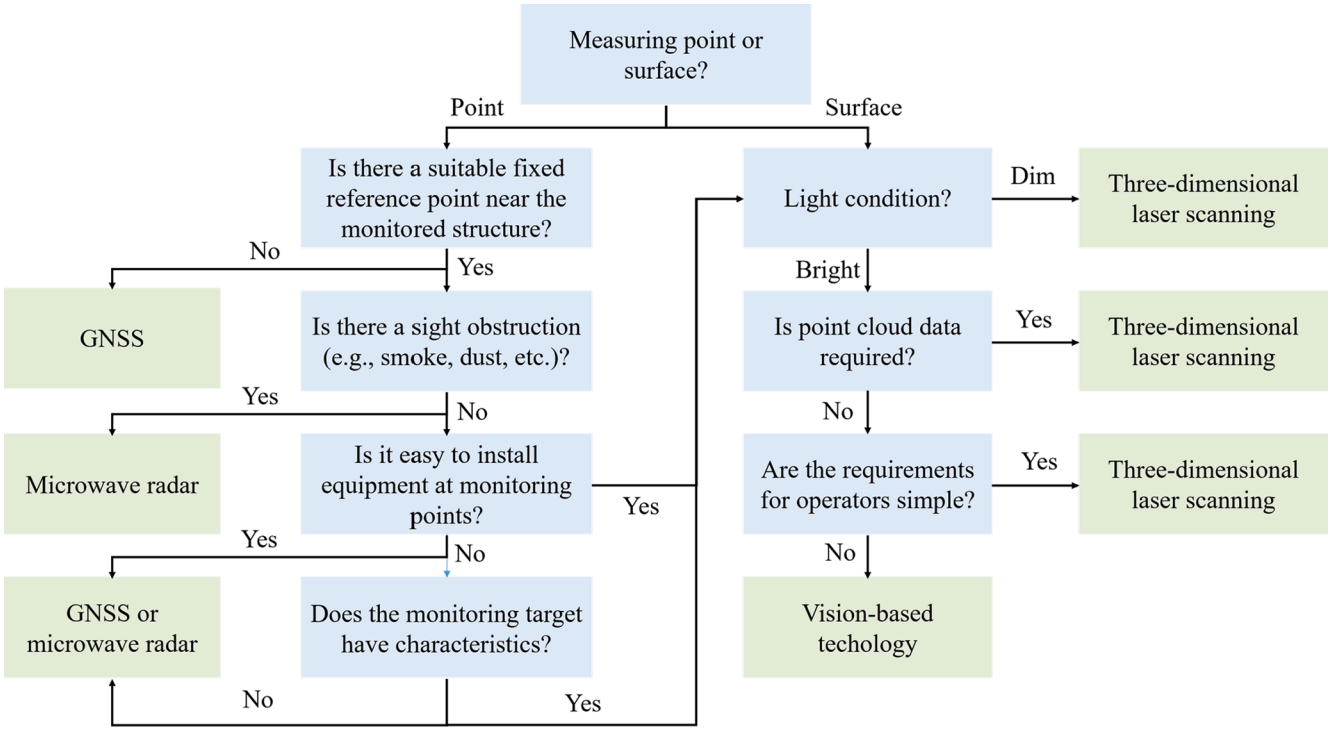

Fig. 15. A decision tree presented to facilitate the selection of appropriate technologies.

can be longer than 145 m. Laser scanning can achieve a measurement frequency up to 200 Hz, and the operation distance can be longer than 2,500 m. Computer vision-based technology can achieve a measurement frequency up to 60 Hz, and the operation distance can be longer than 2,000 m.

- Various effective signal processing algorithms have been developed to improve the measurement accuracy through considering the effects of electromagnetic interference, obstacle shielding (e.g., smoke, dust, cloud, etc.), and the noise of transceiver. With the diverse output data, machine learning methods have been shown effective to improve the measurement performance.
- The reviewed technologies are promising to incorporate autonomous platforms, such as UAV, manned or unmanned aircrafts, and satellite-based platforms. The autonomous platforms can carry sensors and/or instruments to measure distance, thus, significantly improving the mobility and efficiency of measurement.
- Inconsistent statements of the operation distance and robustness of the reviewed technologies can be elucidated by the generation, propagation, and reception of EM waves. The received energy of signals is related to the transmitted power, frequency of EM waves, and reflector property. With certain path attenuation in the propagation of the EM waves and the reflection of the target, the received signals must achieve adequate signal-to-noise ratios, in order to achieve reasonable accuracy.
- A decision tree is proposed to facilitate the selection of distance measurement technologies for intended applications. A suitable selection needs to consider the base station, the obstruction condition of the measured target, the ease of installation, the light condition on the site, the need for integration with BIM, and the operator skills.

Based on this review, the following challenges and future opportunities have been identified to promote further research and development:

- Further research is needed to understand the effects of scattering characteristics of EM waves on the measurement of distance in scenarios involving complex structures and/or dynamic environments. It is envisioned that the measurement accuracy can be further improved based on the further in-depth understandings.
- Effective methods need to be developed to improve the lifecycle cost of the condition assessment system. While different technologies have different measurement performance and limitations in practice, there is a need to develop a method for optimization of the performance and minimize the lifecycle cost. The capability of optimization will help improve the decision making for the selection, operation, and maintenance of the condition assessment system and the management of infrastructure. Promising optimization solutions include various metaheuristic algorithms and machine learning methods.
- Further research and development are needed to improve the installation and long-term operation of the reviewed technologies to facilitate engineering applications. In real-life applications, the performance of the technologies also depends on the requirement of the efforts for deployment, the power supply, the size and the mobility of the instruments required for the measurement.

Declaration of Competing Interest

The authors declare that they have no known competing financial interests or personal relationships that could have appeared to influence the work reported in this paper.

Acknowledgement

This research was funded by Stevens Institute of Technology and U.S. Department of Transportation (award number: 693JK31950008CAAP).

References

[1] American Society of Civil Engineers, America's 2017 infrastructure report card, 2017. https://www.infrastructurereportcard.org/wp-content/uploads/2017/01/Bridges-Final.pdf. Accessed on May 1, 2020.
[2] American Society of Civil Engineers, Failure to Act: Closing the Infrastructure Investment Gap for America's Economic Future, 2016. https://www.asce.org/failuretoact/. Accessed on June 10, 2020.

[3] S. Sony, S. Laventure, A. Sadhu, A literature review of next-generation smart sensing technology in structural health monitoring, Struct. Control Health Monitor. 26 (3) (2019) e2321, https://doi.org/10.1002/stc.2321.
[4] S.A. Dabous, S. Feroz, Condition monitoring of bridges with non-contact testing technologies, Autom. Constr. 116 (2020) 103224, https://doi.org/10.1016/j.autcon.2020.103224.
[5] Y. Bao, V.C. Li, Feasibility study of Lego-inspired construction with bendable concrete, Autom. Constr. 113 (2020) 103161, https://doi.org/10.1016/j.autcon.2020.103161.
[6] F. Craveiroa, J.P. Duartec, H. Bartoloa, P.J. Bartolod, Additive manufacturing as an enabling technology for digital construction: A perspective on Construction 4.0, Autom. Constr. 103 (2019) 251–267, https://doi.org/10.1016/j.autcon.2019.03.011.
[7] P. Carneau, R. Mesnil, N. Roussel, O. Baverel, Additive manufacturing of cantilever-From masonry to concrete 3D printing, Autom. Constr. 116 (2020) 103184, https://doi.org/10.1016/j.autcon.2020.103184.
[8] Q. Lu, L. Chen, S. Li, M. Pitt, Semi-automatic geometric digital twinning for existing buildings based on images and CAD drawings, Autom. Constr. 115 (2020) 103183, https://doi.org/10.1016/j.autcon.2020.103183.
[9] C. Boje, A. Guerriero, S. Kubicki, Y. Rezgui, Towards a semantic construction digital twin: Directions for future research, Autom. Constr. 114 (2020) 103179, https://doi.org/10.1016/j.autcon.2020.103179.
[10] J. Zhou, H. Xiao, W. Jiang, W. Bai, G. Liu, Automatic subway tunnel displacement monitoring using robotic total station, Measurement 151 (2020) 107251, https://doi.org/10.1016/j.measurement.2019.107251.
[11] G. Lee, H.H. Kim, C.J. Lee, S.I. Ham, S.H. Yun, H. Cho, B.K. Kim, G.T. Kim, K. Kim, A laser-technology-based lifting-path tracking system for a robotic tower crane, Autom. Constr. 18 (7) (2009) 865–874, https://doi.org/10.1016/j.autcon.2009.03.011.
[12] L.M. González-deSantos, J. Martínez-Sánchez, H. González-Jorge, F. Navarro-Medina, P. Arias, UAV payload with collision mitigation for contact inspection, Autom. Constr. 115 (2020) 103200, https://doi.org/10.1016/j.autcon.2020.103200.
[13] Y. Zhou, S. Chen, Vehicle ride comfort analysis with whole-body vibration on long-span bridges subjected to crosswind, J. Wind Eng. Ind. Aerodyn. 155 (2016) 126–140, https://doi.org/10.1016/j.jweia.2016.05.001.
[14] P. Misra, S.K. Mohini, S.K. Mishra, ANN-based non-linearity compensator of LVDT sensor for structural health monitoring, in: Proceedings of the 7th ACM Conference on Embedded Networked Sensor Systems, 2009, pp. 363–364, https://doi.org/10.1145/1644038.1644103.
[15] S. Joshi, S.M. Harle, Linear variable differential transducer (LVDT) & its applications in civil engineering, Int. J. Transport. Eng. Technol. 3 (4) (2017) 62–66, https://doi.org/10.11648/j.ijtet.20170304.13.
[16] G. Fu, A.G. Moosa, An optical approach to structural displacement measurement and its application, J. Eng. Mech. 128 (5) (2002) 511–520, https://doi.org/10.1061/(ASCE)0733-9399(2002)128:5(511).
[17] C. Rodrigues, C. Félix, A. Lage, J. Figueiras, Development of a long-term monitoring system based on FBG sensors applied to concrete bridges, Eng. Struct. 32 (8) (2010) 1993–2002, https://doi.org/10.1016/j.engstruct.2010.02.033.
[18] B. Chen, X. Wang, D. Sun, X. Xie, Integrated system of structural health monitoring and intelligent management for a cable-stayed bridge, Sci. World J. 2014 (2014), https://doi.org/10.1155/2014/689471.
[19] H.F. Pei, J.H. Yin, H.H. Zhu, C.Y. Hong, W. Jin, D.S. Xu, Monitoring of lateral displacements of a slope using a series of special fibre Bragg grating-based in-place inclinometers, Meas. Sci. Technol. 23 (2) (2012) 025007, https://doi.org/10.12783/shm2017/14123.
[20] Y.L. Wang, B. Shi, T.L. Zhang, H.H. Zhu, Q. Jie, Q. Sun, Introduction to an FBG-based inclinometer and its application to landslide monitoring, J. Civil Struct. Health Monitor. 5 (5) (2015) 645–653, https://doi.org/10.1007/s13349-015-0129-4.
[21] Y. Bao, Y. Huang, M.S. Hoehler, G. Chen, Review of fiber optic sensors for structural fire engineering, Sensors 19 (4) (2019) 877, https://doi.org/10.3390/s19040877.
[22] A. Parizzi, F. Rodriguez Gonzalez, R. Brcic, A covariance-based approach to merging InSAR and GNSS displacement rate measurements, Remote Sensing 12 (2) (2020) 300, https://doi.org/10.3390/rs12020300.
[23] C. Pipitone, A. Maltese, G. Dardanelli, M. Lo Brutto, G. La Loggia, Monitoring water surface and level of a reservoir using different remote sensing approaches and comparison with dam displacements evaluated via GNSS, Remote Sensing 10 (1) (2018) 71, https://doi.org/10.3390/rs10010071.
[24] D.V. Rodrigues, D. Zuo, Z. Tang, J. Wang, C. Gu, C. Li, Adaptive displacement calibration strategies for field structural health monitoring based on Doppler radars, IEEE Trans. Instrum. Meas. (2020), https://doi.org/10.1109/TIM.2020.2982233.
[25] Y. Xiong, Z. Peng, G. Xing, W. Zhang, G. Meng, Accurate and robust displacement measurement for FMCW radar vibration monitoring, IEEE Sens. J. 18 (3) (2017) 1131–1139, https://doi.org/10.1109/JSEN.2017.2778294.
[26] H.C. Jo, J. Kim, K. Lee, H.G. Sohn, Y.M. Lim, Non-contact strain measurement for laterally loaded steel plate using LiDAR point cloud displacement data, Sens. Actuators, A 283 (2018) 362–374, https://doi.org/10.1016/j.sna.2018.09.012.
[27] K. Kim, H. Sohn, Dynamic displacement estimation by fusing LDV and LiDAR measurements via smoothing based Kalman filtering, Mech. Syst. Sig. Process. 82 (2017) 339–355, https://doi.org/10.1016/j.ymssp.2016.05.027.
[28] X.W. Ye, T.H. Yi, C.Z. Dong, T. Liu, Vision-based structural displacement measurement: System performance evaluation and influence factor analysis, Measurement 88 (2016) 372–384, https://doi.org/10.1016/j.measurement.2016.01.024.
[29] D. Feng, M.Q. Feng, Experimental validation of cost-effective vision-based structural health monitoring, Mech. Syst. Sig. Process. 88 (2017) 199–211, https://doi.org/10.1016/j.ymssp.2016.11.021.
[30] J. Yu, X. Meng, B. Yan, B. Xu, Q. Fan, Y. Xie, Global Navigation Satellite System-based positioning technology for structural health monitoring: A review, Struct. Control Health Monitor. 27 (1) (2020) e2467, https://doi.org/10.1002/stc.2467.
[31] D. Feng, M.Q. Feng, Computer vision for SHM of civil infrastructure: From dynamic response measurement to damage detection–A review, Eng. Struct. 156 (2018) 105–117, https://doi.org/10.1016/j.engstruct.2017.11.018.
[32] NASA, EM Spectrum Properties. Wikimedia, 2007. https://commons.wikimedia.org/wiki/File:EM_Spectrum_Properties_edit.svg. Accessed on June 10, 2020.
[33] G. Petrie, C.K. Toth, Introduction to laser ranging, profiling, and scanning, in: Topographic Laser Ranging and Scanning: Principles and processing, 2008, pp. 1–28, https://doi.org/10.1201/9781315154381-1.
[34] J.W. Lovse, W.F. Teskey, G. Lachapelle, M.E. Cannon, Dynamic deformation monitoring of tall structure using GPS technology, J. Surv. Eng. 121 (1) (1995) 35–40, https://doi.org/10.1061/(ASCE)0733-9453(1995)121:1(35).
[35] Z. Shao, X. Zhang, Y. Li, J. Jiang, A comparative study on radar interferometry for vibrations monitoring on different types of bridges, IEEE Access 6 (2018) 29677–29684, https://doi.org/10.1109/ACCESS.2018.2839688.
[36] C. Li, W. Chen, G. Liu, R. Yan, H. Xu, Y. Qi, A noncontact FMCW radar sensor for displacement measurement in structural health monitoring, Sensors 15 (4) (2015) 7412–7433, https://doi.org/10.3390/s150407412.
[37] D. Erdenebat, D. Waldmann, Application of the DAD method for damage localisation on an existing bridge structure using close-range UAV photogrammetry, Eng. Struct. 218 (2020) 110727, https://doi.org/10.1016/j.engstruct.2020.110727.
[38] O. Frey, C.L. Werner, R. Coscione, Car-borne and UAV-borne mobile mapping of surface displacements with a compact repeat-pass interferometric SAR system at L-band, in: IGARSS 2019-2019 IEEE International Geoscience and Remote Sensing Symposium, 2019, pp. 274–277, https://doi.org/10.1109/IGARSS.2019.8897827.
[39] E.J. Hoppe, F. Novali, A. Rucci, A. Fumagalli, S. Del Conte, G. Falorni, N. Toro, Deformation monitoring of posttensioned bridges using high-resolution satellite remote sensing, J. Bridge Eng. 24 (12) (2019) 04019115, https://doi.org/10.1061/(ASCE)BE.1943-5592.0001479.
[40] J. Yu, P. Zhu, B. Xu, X. Meng, Experimental assessment of high sampling-rate robotic total station for monitoring bridge dynamic responses, Measurement 104 (2017) 60–69, https://doi.org/10.1016/j.measurement.2017.03.014.
[41] B. Halford, Mapping corrosion with hyperspectral imaging, 10–10, C&EN Global Enterprise 96 (41) (2018), https://doi.org/10.1109/10.1021/cen-09641-scicon6.
[42] M.T. Bui, R. Doskočil, V. Krivanek, T.H. Ha, Y.T. Bergeon, P. Kutilek, Indirect method to estimate distance measurement based on single visual cameras, in: 2017 International Conference on Military Technologies (ICMT), 2017, pp. 695–700, https://doi.org/10.1109/MILTECHS.2017.7988846.
[43] D. Jiang, Z. Zheng, G. Li, Y. Sun, J. Kong, G. Jiang, H. Xiong, B. Tao, S. Xu, H. Yu, H. Liu, Gesture recognition based on binocular vision, Cluster Computing 22 (6) (2019) 13261–13271, https://doi.org/10.1007/s10586-018-1844-5.
[44] N. Yamaguti, S. Oe, K. Terada, A method of distance measurement by using monocular camera, in: Proceedings of the 36th SICE Annual Conference, 1997, pp. 1255–1260, https://doi.org/10.1109/SICE.1997.624999.
[45] M.J. Jung, H. Myung, H.K. Lee, S. Bang, Ambiguity resolving in structured light 2D range finder for SLAM operation for home robot applications, in: IEEE Workshop on Advanced Robotics and its Social Impacts, 2005, pp. 18–23, https://doi.org/10.1109/ARSO.2005.1511613.
[46] A. Rashidi, I. Brilakis, P. Vela, Generating absolute-scale point cloud data of built infrastructure scenes using a monocular camera setting, J. Comput. Civil Eng. 29 (6) (2015) 04014089, https://doi.org/10.1061/(ASCE)CP.1943-5487.0000414.
[47] L. Wu, Y. Su, Z. Chen, S. Chen, S. Cheng, P. Lin, Six-degree-of-freedom generalized displacements measurement based on binocular vision, Struct. Control Health Monitor. 27 (2) (2020) e2458, https://doi.org/10.1002/stc.2458.
[48] Y. Zhang, X. Zhao, P. Liu, Multi-point displacement monitoring based on full convolutional neural network and smartphone, IEEE Access 7 (2019) 139628–139634, https://doi.org/10.1109/ACCESS.2019.2943599.
[49] N. Wang, K. Ri, H. Liu, X. Zhao, Structural displacement monitoring using smartphone camera and digital image correlation, IEEE Sens. J. 18 (11) (2018) 4664–4672, https://doi.org/10.1109/JSEN.2018.2828139.
[50] J.M. Franco, J.M. Caicedo, J. Marulanda, M. Sutton, P. Thomson, RGB-D-DIC technique for low-cost 3D displacement fields measurements, Eng. Struct. 197 (2019) 109457, https://doi.org/10.1016/j.engstruct.2019.109457.
[51] Y.L. Chen, M. Abdelbarr, M.R. Jahanshahi, S.F. Masri, Color and depth data fusion using an RGB-D sensor for inexpensive and contactless dynamic displacement-field measurement, Struct. Control Health Monitor. 24 (11) (2017) e2000, https://doi.org/10.1002/stc.2000.
[52] Y. Xu, J.M. Brownjohn, Review of machine-vision based methodologies for displacement measurement in civil structures, J. Civil Struct. Health Monitor. 8 (1) (2018) 91–110, https://doi.org/10.1007/s13349-017-0261-4.
[53] G.W. Roberts, X. Meng, P. Psimoulis, C.J. Brown, Time series analysis of rapid GNSS measurements for quasi-static and dynamic bridge monitoring, Geodetic Time Series Anal. Earth Sci. (2020) 345–417, https://doi.org/10.1007/978-3-030-21718-1_12.
[54] P. Salvatori, C. Stallo, A. Coluccia, F. Rispoli, A. Neri, Differential GNSS and double difference approaches comparison for high integrity railway location determination system, in: 2018 5th IEEE International Workshop on Metrology

for AeroSpace (MetroAeroSpace), 2018, pp. 1–5, https://doi.org/10.1109/MetroAeroSpace.2018.8453615.
[55] R. Xi, W. Jiang, X. Meng, H. Chen, Q. Chen, Bridge monitoring using BDS-RTK and GPS-RTK techniques, Measurement 120 (2018) 128–139, https://doi.org/10.1016/j.measurement.2018.02.001.
[56] H. Jo, S.H. Sim, A. Tatkowski, B.F. Spencer Jr, M.E. Nelson, Feasibility of displacement monitoring using low-cost GPS receivers, Struct. Control Health Monitor. 20 (9) (2013) 1240–1254, https://doi.org/10.1002/stc.1532.
[57] M. Su, J. Zheng, Y. Yang, Q. Wu, A new multipath mitigation method based on adaptive thresholding wavelet denoising and double reference shift strategy, GPS Solut. 22 (2) (2018) 40, https://doi.org/10.1007/s10291-018-0708-z.
[58] J. Yu, B. Yan, X. Meng, X. Shao, H. Ye, Measurement of bridge dynamic responses using network-based real-time kinematic GNSS technique, J. Surv. Eng. 142 (3) (2016) 04015013, https://doi.org/10.1061/(ASCE)SU.1943-5428.0000167.
[59] M.R. Kaloop, D. Kim, De-noising of GPS structural monitoring observation error using wavelet analysis, Geomatics, Natural Hazards Risk 7 (2) (2016) 804–825, https://doi.org/10.1080/19475705.2014.983186.
[60] M.R. Kaloop, C.O. Yigit, A. El-Mowafy, A.A. Dindar, M. Bezcioglu, J.W. Hu, Hybrid wavelet and principal component analyses approach for extracting dynamic motion characteristics from displacement series derived from multipath-affected high-rate GNSS observations, Remote Sensing 12 (1) (2020) 79, https://doi.org/10.3390/rs12010079.
[61] C. Xiong, H. Lu, J. Zhu, Operational modal analysis of bridge structures with data from GNSS/accelerometer measurements, Sensors 17 (3) (2017) 436, https://doi.org/10.3390/s17030436.
[62] I. Peppa, P. Psimoulis, X. Meng, Using the signal-to-noise ratio of GPS records to detect motion of structures, Struct. Control Health Monitor. 25 (2) (2018) e2080, https://doi.org/10.1002/stc.2080.
[63] W. Guo, G. Wang, Y. Bao, P. Li, M. Zhang, Q. Gong, R. Li, Y. Gao, R. Zhao, S. Shen, Detection and monitoring of tunneling-induced riverbed deformation using GPS and BeiDou: A Case Study, Appl. Sci. 9 (13) (2019) 2759, https://doi.org/10.3390/app9132759.
[64] M.R. Kaloop, D. Kim, GPS-structural health monitoring of a long span bridge using neural network adaptive filter, Survey Rev. 46 (334) (2014) 7–14, https://doi.org/10.1179/1752270613Y.0000000053.
[65] Y. Quan, L. Lau, G.W. Roberts, X. Meng, C. Zhang, Convolutional neural network based multipath detection method for static and kinematic GPS high precision positioning, Remote Sensing 10 (12) (2018) 2052, https://doi.org/10.3390/rs10122052.
[66] M.R. Kaloop, M. Hussan, D. Kim, Time-series analysis of GPS measurements for long-span bridge movements using wavelet and model prediction techniques, Adv. Space Res. 63 (11) (2019) 3505–3521, https://doi.org/10.1016/j.asr.2019.02.027.
[67] M. Hussan, M.R. Kaloop, F. Sharmin, D. Kim, GPS performance assessment of cable-stayed bridge using wavelet transform and Monte-Carlo techniques, KSCE J. Civ. Eng. 22 (11) (2018) 4385–4398, https://doi.org/10.1007/s12205-018-0438-3.
[68] T. Kumberg, S. Schneid, L. Reindl, A wireless sensor network using GNSS receivers for a short-term assessment of the modal properties of the Neckartal bridge, Appl. Sci. 7 (6) (2017) 626, https://doi.org/10.3390/app7060626.
[69] R. Xiao, H. Shi, X. He, Z. Li, D. Jia, Z. Yang, Deformation monitoring of reservoir dams using GNSS: An application to south-to-north water diversion project, China, IEEE Access 7 (2019) 54981–54992, https://doi.org/10.1109/ACCESS.2019.2912143.
[70] R. Xi, X. Meng, W. Jiang, Q. He, X. An, Performance analysis of bridge monitoring with the integrated GPS, BDS and GLONASS, in: 4th Joint International Symposium on Deformation Monitoring (JISDM), 2019, https://jisdm2019.org/wp-content/uploads/2019/05/47.pdf.
[71] K. Kim, J. Choi, J. Chung, G. Koo, I.H. Bae, H. Sohn, Structural displacement estimation through multi-rate fusion of accelerometer and RTK-GPS displacement and velocity measurements, Measurement 130 (2018) 223–235, https://doi.org/10.1016/j.measurement.2018.07.090.
[72] L. Piotrowsky, T. Jaeschke, S. Kueppers, J. Siska, N. Pohl, Enabling high accuracy distance measurements with FMCW radar sensors, IEEE Trans. Microw. Theory Tech. 67 (12) (2019) 5360–5371, https://doi.org/10.1109/TMTT.2019.2930504.
[73] A.C. Amies, C.G. Pretty, G.W. Rodgers, J.G. Chase, Experimental validation of a radar-based structural health monitoring system, IEEE/ASME Trans. Mechatron. 24 (5) (2019) 2064–2072, https://doi.org/10.1109/TMECH.2019.2934091.
[74] O.D. Winarko, R. Hidayat, H.A. Nugroho, R. Anggara, A.A. Lestari, Mitigation methods of sawtooth modulations effect on FMCW radar INDERA MX-4, in: 2017 International Conference on Radar, Antenna, Microwave, Electronics, and Telecommunications (ICRAMET), 2017, pp. 42–46, https://doi.org/10.1109/ICRAMET.2017.8253142.
[75] A.C. Amies, C.G. Pretty, G.W. Rodgers, J.G. Chase, Shake table testing of a radar-based structural health monitoring method, in: 14th IEEE/ASME International Conference on Mechatronic and Embedded Systems and Applications, 2018, pp. 1–6, https://doi.org/10.1109/MESA.2018.8449179.
[76] Y. Bao, M.T. Ghasr, K. Ying, G. Chen, R. Zoughi, Microwave synthetic aperture radar imaging for nondestructive evaluation of mechanically stabilized earth walls, in: Unknown (Ed.), Materials Evaluation 75(2), American Society for Nondestructive Testing, 2017, pp. 177–184, https://ndtlibrary.asnt.org/2017/MicrowaveSyntheticApertureRadarImagingforNondestructiveEvaluationofMechanicallyStabilizedEarthWal.
[77] Y. Bao, M.T. Ghasr, K. Ying, G. Chen, R. Zoughi, Evaluation of Mechanically Stabilized Earth Walls with Microwave Synthetic Aperture Radar Imaging, in: Unknown (Ed.), Journal of Geotechnical and Geoenvironmental Engineering 143 (5), ASCE, 2017, p. 02816002, https://doi.org/10.1061/(ASCE)GT.1943-5606.0001639.
[78] S. Melo, S. Maresca, S. Pinna, F. Scotti, M. Khosravanian, C.S. Arismar, F. Giannetti, A.D. Barman, A. Bogoni, Photonics-based dual-band radar for landslides monitoring in presence of multiple scatterers, J. Lightwave Technol. 36 (12) (2018) 2337–2343, https://doi.org/10.1109/JLT.2018.2814638.
[79] S. Melo, S. Maresca, S. Pinna, F. Scotti, M. Khosravanian, A.C. S Jr, F. Giannetti, A.D. Barmann, A. Bogoni, High precision displacement measurements in presence of multiple scatterers using a photonics-based dual-band radar, International Conference on Radar Systems (Radar 2017), 2017, pp.1–6. https://doi.org/10.1049/cp.2017.0413.
[80] M. Maizuar, L. Zhang, S. Miramini, P. Mendis, C. Duffield, Structural health monitoring of bridges using advanced non-destructive testing technique, ACMSM25, 2020, pp. 963–972. https://doi.org/10.1007/978-981-13-7603-0_91.
[81] A.B. Suksmono, A. Munir, Signal processing of range detection for SFCW radars using Matlab and GNU radio, in: 2014 International Conference on Computer, Control, Informatics and Its Applications (IC3INA), 2014, pp. 145–148, https://doi.org/10.1109/IC3INA.2014.7042617.
[82] A. Budillon, G. Ferraioli, A.C. Johnsy, V. Pascazio, G. Schirinzi, TomoSAR application for early warning in infrastructure health monitoring, in: IGARSS 2019-2019 IEEE International Geoscience and Remote Sensing Symposium, 2019, pp. 3621–3624, https://doi.org/10.1109/IGARSS.2019.8898674.
[83] X. Qin, L. Zhang, M. Yang, H. Luo, M. Liao, X. Ding, Mapping surface deformation and thermal dilation of arch bridges by structure-driven multi-temporal DInSAR analysis, Remote Sens. Environ. 216 (2018) 71–90, https://doi.org/10.1016/j.rse.2018.06.032.
[84] A.S. Venkatachalam, X. Xu, D. Huston, T. Xia, Development of a new high speed dual-channel impulse ground penetrating radar, IEEE J. Sel. Top. Appl. Earth Obs. Remote Sens. 7 (3) (2013) 753–760, https://doi.org/10.1109/JSTARS.2013.2280995.
[85] H. Cui, X. Ren, Q. Mao, Q. Hu, W. Wang, Shield subway tunnel deformation detection based on mobile laser scanning, Autom. Constr. 106 (2019) 102889, https://doi.org/10.1016/j.autcon.2019.102889.
[86] X. Xu, J. Bureick, H. Yang, I. Neumann, TLS-based composite structure deformation analysis validated with laser tracker, Compos. Struct. 202 (2018) 60–65, https://doi.org/10.1016/j.compstruct.2017.10.015.
[87] H. Yang, X. Xu, I. Neumann, Deformation behavior analysis of composite structures under monotonic loads based on terrestrial laser scanning technology, Compos. Struct. 183 (2018) 594–599, https://doi.org/10.1016/j.compstruct.2017.07.011.
[88] X. Xu, B. Kargoll, J. Bureick, H. Yang, H. Alkhatib, I. Neumann, TLS-based profile model analysis of major composite structures with robust B-spline method, Compos. Struct. 184 (2018) 814–820, https://doi.org/10.1016/j.compstruct.2017.10.057.
[89] X. Xie, X. Lu, Development of a 3D modeling algorithm for tunnel deformation monitoring based on terrestrial laser scanning, Underground Space 2 (1) (2017) 16–29, https://doi.org/10.1016/j.undsp.2017.02.001.
[90] B. Riveiro, M.J. DeJong, B. Conde, Automated processing of large point clouds for structural health monitoring of masonry arch bridges, Autom. Constr. 72 (2016) 258–268, https://doi.org/10.1016/j.autcon.2016.02.009.
[91] Y.Q. Ni, Y.W. Wang, W.Y. Liao, W.H. Chen, A vision-based system for long-distance remote monitoring of dynamic displacement: Experimental verification on a supertall structure, Smart Struct. Syst. 24 (6) (2019) 769–781, https://doi.org/10.12989/sss.2019.24.6.769.
[92] C.Z. Dong, O. Celik, F.N. Catbas, Marker-free monitoring of the grandstand structures and modal identification using computer vision methods, Struct. Health Monitor. 18 (5–6) (2019) 1491–1509, https://doi.org/10.1177/1475921718806895.
[93] P. Xiao, Z.Y. Wu, R. Christenson, S. Lobo-Aguilar, Development of video analytics with template matching methods for using camera as sensor and application to highway bridge structural health monitoring. Journal of Civil, Struct. Health Monitor. (2020) 1–20, https://doi.org/10.1007/s13349-020-00392-6.
[94] L. He, J. Tan, Q. Hu, S. He, Q. Cai, Y. Fu, S. Tang, Non-contact measurement of the surface displacement of a slope based on a smart binocular vision system, Sensors 18 (9) (2018) 2890, https://doi.org/10.3390/s18092890.
[95] J.M.W. Brownjohn, Y. Xu, D. Hester, Vision-based bridge deformation monitoring, Front. Built Environ. 3 (2017) 23, https://doi.org/10.3389/fbuil.2017.00023.
[96] I.H. Chen, S.C. Ho, M.B. Su, Computer vision application programming for settlement monitoring in a drainage tunnel, Autom. Constr. 110 (2020) 103011, https://doi.org/10.1016/j.autcon.2019.103011.
[97] C.Z. Dong, O. Celik, F.N. Catbas, E.J. O'Brien, S. Taylor, Structural displacement monitoring using deep learning-based full field optical flow methods, Struct. Infrastruct. Eng. 16 (1) (2020) 51–71, https://doi.org/10.1080/15732479.2019.1650078.
[98] C.Z. Dong, F.N. Catbas, A non-target structural displacement measurement method using advanced feature matching strategy, Adv. Struct. Eng. 22 (16) (2019) 3461–3472, https://doi.org/10.1177/1369433219856171.
[99] Y. Xu, J. Brownjohn, D. Kong, A non-contact vision-based system for multipoint displacement monitoring in a cable-stayed footbridge, Struct. Control Health Monitor. 25 (5) (2018) e2155, https://doi.org/10.1002/stc.2155.
[100] L. Luo, M.Q. Feng, J. Wu, A comprehensive alleviation technique for optical-turbulence-induced errors in vision-based displacement measurement, Struct. Control Health Monitor. 27 (3) (2020) e2496, https://doi.org/10.1002/stc.2496.

[101] D. Feng, M.Q. Feng, Vision-based multipoint displacement measurement for structural health monitoring, Struct. Control Health Monitor. 23 (5) (2016) 876–890, https://doi.org/10.1002/stc.1819.
[102] E. Ilg, N. Mayer, T. Saikia, M. Keuper, A. Dosovitskiy, T. Brox, Flownet 2.0: Evolution of optical flow estimation with deep networks, in: Proceedings of the IEEE conference on computer vision and pattern recognition, 2017, pp. 2462–2470, https://doi.org/10.1109/CVPR.2017.179.
[103] S. Shirowzhan, S.M. Sepasgozar, H. Li, J. Trinder, P. Tang, Comparative analysis of machine learning and point-based algorithms for detecting 3D changes in buildings over time using bi-temporal lidar data, Autom. Constr. 105 (2019) 102841, https://doi.org/10.1016/j.autcon.2019.102841.
[104] F. Huang, J. Huang, S. Jiang, C. Zhou, Landslide displacement prediction based on multivariate chaotic model and extreme learning machine, Eng. Geol. 218 (2017) 173–186, https://doi.org/10.1016/j.enggeo.2017.01.016.
[105] Q. Fan, X. Meng, D.T. Nguyen, Y. Xie, J. Yu, Predicting displacement of bridge based on CEEMDAN-KELM model using GNSS monitoring data, J. Appl. Geodesy 1 (2020), https://doi.org/10.1515/jag-2019-0057.
[106] N. Anantrasirichai, J. Biggs, F. Albino, P. Hill, D. Bull, Application of machine learning to classification of volcanic deformation in routinely generated InSAR data, J. Geophys. Res. Solid Earth 123 (8) (2018) 6592–6606, https://doi.org/10.1029/2018JB015911.
[107] S. Valade, A. Ley, F. Massimetti, O. D'Hondt, M. Laiolo, D. Coppola, D. Loibl, O. Hellwich, T.R. Walter, Towards global volcano monitoring using multisensor sentinel missions and artificial intelligence: The mounts monitoring system, Remote Sensing 11 (13) (2019) 1528, https://doi.org/10.3390/rs11131528.
[108] N. Anantrasirichai, J. Biggs, F. Albino, D. Bull, The application of convolutional neural networks to detect slow, sustained deformation in InSAR time series, Geophys. Res. Lett. 46 (21) (2019) 11850–11858, https://doi.org/10.1029/2019GL084993.
[109] X. Xu, H. Yang, Robust model reconstruction for intelligent health monitoring of tunnel structures, 1729881420910836, Int. J. Adv. Rob. Syst. 17 (2) (2020), https://doi.org/10.1177/1729881420910836.
[110] M. Wojtkowska, M. Kedzierski, P. Delis, Validation of terrestrial laser scanning and artificial intelligence for measuring deformations of cultural heritage structures, Measurement 167 (2021) 108291, https://doi.org/10.1016/j.measurement.2020.108291.
[111] Y. Zhang, P. Liu, X. Zhao, Structural displacement monitoring based on mask regions with convolutional neural network, Constr. Build. Mater. (2020) 120923, https://doi.org/10.1016/j.conbuildmat.2020.120923.
[112] R. Yang, S.K. Singh, M. Tavakkoli, N. Amiri, Y. Yang, M.A. Karami, R. Rai, CNN-LSTM deep learning architecture for computer vision-based modal frequency detection, Mech. Syst. Sig. Process. 144 (2020) 106885, https://doi.org/10.1016/j.ymssp.2020.106885.
[113] H. Luo, S.G. Paal, A locally weighted machine learning model for generalized prediction of drift capacity in seismic vulnerability assessments, Comput.-Aided Civ. Infrastruct. Eng. 34 (11) (2019) 935–950, https://doi.org/10.1111/mice.12456.
[114] J.V.M. de Oliveira, A.P.C. Larocca, J.O. de Araújo Neto, A.L. Cunha, M.C. dos Santos, R.E. Schaal, Vibration monitoring of a small concrete bridge using wavelet transforms on GPS data, J. Civil Struct. Health Monitor. 9 (3) (2019) 397–409, https://doi.org/10.1007/s13349-019-00341-y.
[115] M. Maizuar, L. Zhang, S. Miramini, P. Mendis, R.G. Thompson, Detecting structural damage to bridge girders using radar interferometry and computational modelling, Struct. Control Health Monitor. 24 (10) (2017) e1985, https://doi.org/10.1002/stc.1985.
[116] N.T. Kien, S. Nakashima, N. Shimizu, Displacement monitoring using GPS at an unstable steep slope and the performance of a new low-cost GPS sensor, Geotech. Sustainable Infrastruct. Develop. (2020) 1197–1202, https://doi.org/10.1007/978-981-15-2184-3_157.
[117] P. Górski, Dynamic characteristic of tall industrial chimney estimated from GPS measurement and frequency domain decomposition, Eng. Struct. 148 (2017) 277–292, https://doi.org/10.1016/j.engstruct.2017.06.066.
[118] K. Kim, J. Choi, G. Ko, J. Chung, H. Sohn, Structural displacement, velocity and acceleration measurement system based on accelerometer and GPS-RTK for large-scale civil structures, Struct. Health Monitor. 2017 (2017), https://doi.org/10.12783/shm2017/14123.
[119] G. Zhang, Y. Wu, W. Zhao, J. Zhang, Radar-based multipoint displacement measurements of a 1200-m-long suspension bridge, ISPRS J. Photogramm. Remote Sens. 167 (2020) 71–84, https://doi.org/10.1016/j.isprsjprs.2020.06.017.
[120] W. Zhao, G. Zhang, J. Zhang, Cable force estimation of a long-span cable-stayed bridge with microwave interferometric radar, Comput.-Aided Civ. Infrastruct. Eng. 35 (12) (2020) 1419–1433, https://doi.org/10.1111/mice.12557.
[121] S. Guan, J.A. Rice, C. Li, Y. Li, G. Wang, Structural displacement measurements using DC coupled radar with active transponder, Struct. Control Health Monitor. 24 (4) (2017) e1909, https://doi.org/10.1002/stc.1909.
[122] T. Owerko, P. Kuras, Effective processing of radar data for bridge damage detection, Shock Vib. 2019 (2019), https://doi.org/10.1155/2019/2621092.
[123] C. Negulescu, G. Luzi, M. Crosetto, D. Raucoules, A. Roullé, D. Monfort, L. Pujades, B. Colas, T. Dewez, Comparison of seismometer and radar measurements for the modal identification of civil engineering structures, Eng. Struct. 51 (2013) 10–22, https://doi.org/10.1016/j.engstruct.2013.01.005.
[124] G. Luzi, M. Crosetto, E. Fernández, Radar interferometry for monitoring the vibration characteristics of buildings and civil structures: Recent case studies in Spain, Sensors 17 (4) (2017) 669, https://doi.org/10.3390/s17040669.
[125] Q. Huang, G. Luzi, O. Monserrat, M. Crosetto, Ground-based synthetic aperture radar interferometry for deformation monitoring: a case study at Geheyan Dam, China, J. Appl. Remote Sens. 11 (3) (2017) 036030, https://doi.org/10.1117/1.JRS.11.036030.
[126] J. Lee, K.C. Lee, S. Lee, Y.J. Lee, S.H. Sim, Long-term displacement measurement of bridges using a LiDAR system, Struct. Control Health Monitor. 26 (10) (2019) e2428, https://doi.org/10.1002/stc.2428.
[127] J. Erdélyi, A. Kopáčik, I. Lipták, P. Kyrinovič, Automation of point cloud processing to increase the deformation monitoring accuracy, Appl. Geomat. 9 (2) (2017) 105–113, https://doi.org/10.1007/s12518-017-0186-y.
[128] P. Oskouie, B. Becerik-Gerber, L. Soibelman, Automated measurement of highway retaining wall displacements using terrestrial laser scanners, Autom. Constr. 65 (2016) 86–101, https://doi.org/10.1016/j.autcon.2015.12.023.
[129] E. Friedli, R. Presl, A. Wieser, Influence of atmospheric refraction on terrestrial laser scanning at long range, in: Proceedings of the 4th Joint International Symposium on Deformation Monitoring (JISDM), 2019, pp. 15–17. https://jisdm2019.org/wp-content/uploads/2019/05/18.pdf.
[130] L. Zhang, P. Liu, X. Yan, X. Zhao, Middle displacement monitoring of medium–small span bridges based on laser technology, Struct. Control Health Monitor. 27 (4) (2020) e2509, https://doi.org/10.1002/stc.2509.
[131] H. Yoon, J. Shin, B.F. Spencer Jr, Structural displacement measurement using an unmanned aerial system, Comput.-Aided Civ. Infrastruct. Eng. 33 (3) (2018) 183–192, https://doi.org/10.1111/mice.12338.
[132] J. Lee, K.C. Lee, S. Jeong, Y.J. Lee, S.H. Sim, Long-term displacement measurement of full-scale bridges using camera ego-motion compensation, Mech. Syst. Sig. Process. 140 (2020) 106651, https://doi.org/10.1016/j.ymssp.2020.106651.
[133] Y. Yang, X. Sang, S. Yang, X. Hou, Y. Huang, High-precision vision sensor method for dam surface displacement measurement, IEEE Sens. J. 19 (24) (2019) 12475–12481, https://doi.org/10.1109/JSEN.2019.2940069.
[134] J. Li, B. Xie, X. Zhao, Measuring the interstory drift of buildings by a smartphone using a feature point matching algorithm, Struct. Control Health Monitor. 27 (4) (2020) e2492, https://doi.org/10.1002/stc.2492.
[135] F. Rodriguez-Morales, E. Arnold, R. Hale, S. Keshmiri, C. Leuschen, J. Li, J. Paden, Multi-spectral radar measurements of ice and snow using manned and unmanned aircraft, in: First IEEE International Symposium of Geoscience and Remote Sensing, 2017, pp. 1–4, https://doi.org/10.1109/GRSS-CHILE.2017.7996024.
[136] J. Li, F. Rodriguez-Morales, E. Arnold, C. Leuschen, J. Paden, J. Shang, D. Gomez-Garcia, C. Larsen, Airborne snow measurements over Alaska mountains and glaciers with a compact FMCW radar, in: IGARSS 2019-2019 IEEE International Geoscience and Remote Sensing Symposium, 2019, pp. 3906–3909, https://doi.org/10.1061/10.1109/IGARSS.2019.8900034.
[137] F. Jalinoos, M. Amjadian, A.K. Agrawal, C. Brooks, D. Banach, Experimental evaluation of unmanned aerial system for measuring bridge movement, J. Bridge Eng. 25 (1) (2020) 04019132, https://doi.org/10.1061/(ASCE)BE.1943-5592.0001508.
[138] Y. Tian, C. Zhang, S. Jiang, J. Zhang, W. Duan, Noncontact cable force estimation with unmanned aerial vehicle and computer vision, Comput.-Aided Civ. Infrastruct. Eng. (2020), https://doi.org/10.1111/mice.12567.
[139] X. Wang, C.E. Wittich, T.C. Hutchinson, Y. Bock, D. Goldberg, E. Lo, F. Kuester, Methodology and validation of UAV-based video analysis approach for tracking earthquake-induced building displacements, J. Comput. Civil Eng. 34 (6) (2020) 04020045, https://doi.org/10.1061/(ASCE)CP.1943-5487.0000928.
[140] T. Khuc, T.A. Nguyen, H. Dao, F.N. Catbas, Swaying displacement measurement for structural monitoring using computer vision and an unmanned aerial vehicle, in: Measurement, 2020, p. 107769, https://doi.org/10.1016/j.measurement.2020.107769.
[141] K. Li, J. Wang, D. Qi, The development and application of an original 3D laser scanning: a precise and nondestructive structural measurements system, Frattura ed Integrità Strutturale 14 (51) (2020) 386–397, https://doi.org/10.3221/IGF-ESIS.51.28.
[142] M. Pejić, V. Ogrizović, B. Božić, B. Milovanović, S. Marošan, A simplified procedure of metrological testing of the terrestrial laser scanners, Measurement 53 (2014) 260–269, https://doi.org/10.1016/j.measurement.2014.03.024.
[143] X. Qin, M. Liao, L. Zhang, M. Yang, Structural health and stability assessment of high-speed railways via thermal dilation mapping with time-series InSAR analysis, IEEE J. Sel. Top. Appl. Earth Obs. Remote Sens. 10 (6) (2017) 2999–3010, https://doi.org/10.1109/JSTARS.2017.2719025.
[144] G. Appleby, J. Rodríguez, Z. Altamimi, Assessment of the accuracy of global geodetic satellite laser ranging observations and estimated impact on ITRF scale: estimation of systematic errors in LAGEOS observations 1993–2014, J. Geod. 90 (12) (2016) 1371–1388, https://doi.org/10.1007/s00190-016-0929-2.
[145] P. Milillo, D. Tapete, F. Cigna, D. Perissin, J. Salzer, P. Lundgren, E. Fielding, R. Burgmann, F. Biondi, G. Milillo, C. Serio, Structural health monitoring of engineered structures using a space-borne synthetic aperture radar multi-temporal approach: From cultural heritage sites to war zones, SAR Image Anal., Model., Techn. XVI 10003 (2016) 100030N, https://doi.org/10.1109/JSTARS.2013.2280995.
[146] M.C. Budge, S.R. German, Basic RADAR analysis, Artech House, 2020, ISBN: 9781630815554. https://books.google.com/books?id=_D8szQEACAAJ.
[147] J.A. Shaw, Radiometry and the Friis transmission equation, Am. J. Phys. 81 (1) (2013) 33–37, https://doi.org/10.1119/1.4755780.
[148] J.M. Rius, M. Ferrando, L. Jofre, High-frequency RCS of complex radar targets in real-time, IEEE Trans. Antennas Propag. 41 (9) (1993) 1308–1319, https://doi.org/10.1109/8.247759.

[149] C.G. Someda, Electromagnetic waves, Taylor & Francis, 1998, ISBN: 9780412578700. URL: https://books.google.de/books?id=ENDw-dyLf2sC. Accessed on July 1, 2020.
[150] T. Wang, C.S. Ruf, B. Block, D.S. McKague, S. Gleason, Design and performance of a GPS constellation power monitor system for improved CYGNSS L1B calibration, IEEE J. Sel. Top. Appl. Earth Obs. Remote Sens. 12 (1) (2018) 26–36, https://doi.org/10.1109/JSTARS.2018.2867773.
[151] A. Shrestha, J. Dang, K. Nakajima, X. Wang, Image processing–based real-time displacement monitoring methods using smart devices, Struct. Control Health Monitor. 27 (2) (2020) e2473, https://doi.org/10.1002/stc.2473.
[152] H. Han, J. Wang, X. Meng, H. Liu, Analysis of the dynamic response of a long span bridge using GPS/accelerometer/anemometer under typhoon loading, Eng. Struct. 122 (2016) 238–250, https://doi.org/10.1016/j.engstruct.2016.04.041.
[153] W. Qiu, Y.J. Cheng, High-resolution DEM generation of railway tunnel surface using terrestrial laser scanning data for clearance inspection, J. Comput. Civil Eng. 31 (1) (2017) 04016045, https://doi.org/10.1061/(asce)cp.1943-5487.0000611.
[154] B. LeBlanc, C. Niezrecki, P. Avitabile, J. Chen, J. Sherwood, Damage detection and full surface characterization of a wind turbine blade using three-dimensional digital image correlation, Struct. Health Monitor. 12 (5–6) (2013) 430–439, https://doi.org/10.1177/1475921713506766.
[155] M. Shao, X. Sui, Study on differential GPS positioning methods, in: International Conference on Computer Science and Mechanical Automation (CSMA), 2015, pp. 223–225, https://doi.org/10.1109/CSMA.2015.51.
[156] S. Dawoud, GNSS principles and comparison, Potsdam University, 2012. https://www.snet.tu-berlin.de/fileadmin/fg220/courses/WS1112/snet-project/gnss-principles-and-comparison_dawoud.pdf.
[157] D. Lyu, F. Zeng, X. Ouyang, H. Zhang, Real-time clock comparison and monitoring with multi-GNSS precise point positioning: GPS, GLONASS and Galileo, Adv. Space Res. 65 (1) (2020) 560–571, https://doi.org/10.1016/j.asr.2019.10.029.
[158] P. Poozesh, A. Sabato, A. Sarrafi, C. Niezrecki, P. Avitabile, R. Yarala, Multicamera measurement system to evaluate the dynamic response of utility-scale wind turbine blades, Wind Energy 23 (7) (2020) 1619–1639, https://doi.org/10.1002/we.2505.